Seasonal fluctuations of the rusty carbon sink in thawing permafrost peatlands

*Monique S. Patzner[1], Nora Kainz[1], Erik Lundin[2], Maximilian Barczok[3], Chelsea Smith[4], Elizabeth Herndon[5], Lauren Kinsman-Costello[4], Stefan Fischer[6], Daniel Straub[7,8], Sara Kleindienst[7], Andreas Kappler[1,9] & Casey Bryce[10]**

[1]*Geomicrobiology, Center for Applied Geosciences, University of Tuebingen, Schnarrenbergstrasse 94-96, 72076 Tuebingen, Germany.*

[2]*Swedish Polar Research Secretariat, Abisko Scientific Research Station, Abisko, Vetenskapens väg 38, 98107 Abisko, Sweden.*

[3]*Department of Geology, Kent State University, Kent, OH, 44242, US.*

[4]*Department of Biological Sciences, Kent State University, Kent, OH, 44242, US.*

[5]*Environmental Sciences Division, Oak Ridge National Laboratory, 1 Bethel Valley Rd, Oak Ridge, TN 37830, US.*

[6]*Tuebingen Structural Microscopy Core Facility, Center for Applied Geosciences, University Tuebingen, Schnarrenbergstrasse 94-96, 72076 Tuebingen, Germany.*

[7]*Microbial Ecology, Center for Applied Geosciences, University Tuebingen, Schnarrenbergstrasse 94-96, 72076 Tuebingen, Germany.*

[8]*Quantitative Biology Center (QBiC), University Tuebingen, Auf der Morgenstelle 10, 72076 Tuebingen, Germany.*

[9]*Cluster of Excellence: EXC 2124: Controlling Microbes to Fight Infection, Tübingen, Germany.*

[10]*School of Earth Sciences, University of Bristol, Bristol, UK.*

**Corresponding Author: Casey Bryce*

School of Earth Science, Wills Memorial Building, University of Bristol, Queens Road, Bristol, BS8 1RJ, UK.

Email: casey.bryce@bristol.ac.uk

KEYWORDS: Soil organic carbon, iron, bioavailability, permafrost collapse, seasonal fluctuations, microbial Fe(III) reduction and Fe(II) oxidation, Abisko, Arctic

ABSTRACT

In permafrost peatlands, up to 20% of total organic carbon (OC) is bound to reactive iron (Fe) minerals in the active layer overlying intact permafrost, potentially protecting OC from microbial degradation and transformation into greenhouse gases (GHG) such as CO_2 and CH_4. During the summer, shifts in runoff and soil moisture influence redox conditions and therefore the balance of Fe oxidation and reduction. Whether this "rusty carbon sink" is stable or continuously dissolved by Fe(III) reduction and reformed by Fe(II) oxidation during redox shifts remains unknown. We exposed ferrihydrite (FH)-coated sand in the active layer along a permafrost thaw gradient in Stordalen mire (Abisko, Sweden) over the summer (June to September) to capture changes in redox conditions and quantify formation and dissolution of reactive Fe(III) (oxyhydr)oxides and associated OC. We found that Fe(III) minerals formed under the constantly oxic conditions in palsa soils overlying intact permafrost over the full summer season. In contrast, in fully-thawed fen areas, conditions were continuously anoxic and by late summer 50.4% of the original Fe(III) (oxyhydr)oxides were lost via dissolution while 44.7% and 4.9% of the Fe remained as Fe(III) and Fe(II) on the sand, respectively. Periodic redox shifts (from 0 mV to +300 mV) were observed over the summer season in the partially-thawed bog due to changes in active layer depth, runoff and soil moisture. This resulted in dissolution and loss of 47.5% of initial Fe(III) (oxyhydr)oxides and release of associated OC in early summer when conditions are wetter and more reduced, and new formation of Fe(III) minerals (34.7% gain in comparison to initial Fe) in the late summer under more dry and oxic conditions which again sequestered Fe-bound organic carbon. Our data suggests that the so-called rusty carbon sink is seasonally dynamic in partially-thawed permafrost peatlands, thus likely either promoting or suppressing carbon mineralization and leading to seasonal changes in GHG emissions.

26 GRAPHICAL ABSTRACT

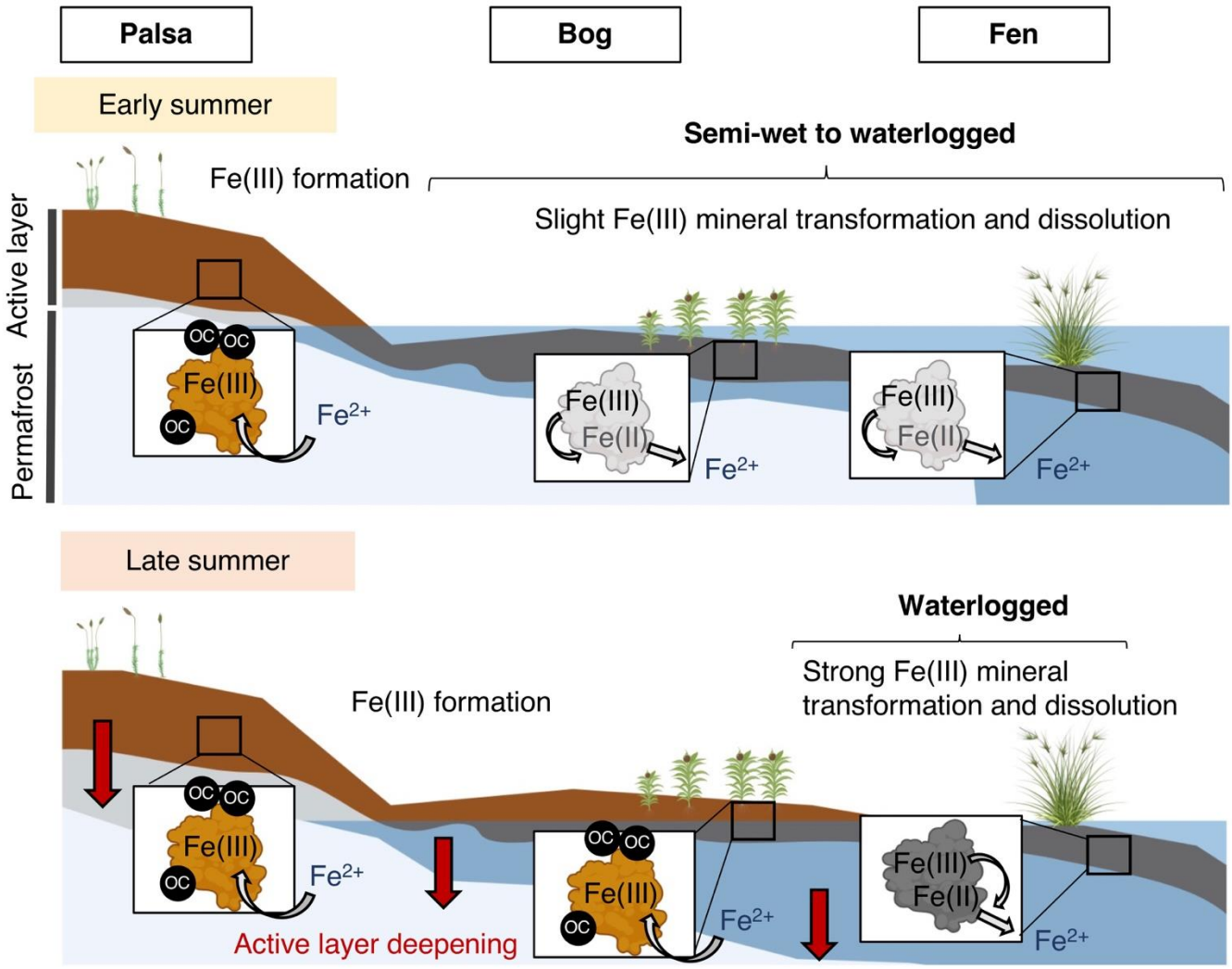

27

28 SYNOPSIS

29 Reactive iron minerals trap or release significant amounts of organic carbon depending on

30 seasonal redox shifts in partially-thawed permafrost peatlands.

INTRODUCTION

Permafrost peatlands hold enormous amounts of organic carbon (OC), equivalent to over one-third of the carbon currently in the atmosphere (~800 Pg)[1, 2]. By the end of this century, permafrost peatlands are predicted to warm from an annual average air temperature below 2°C to between +5.6 to +12.4°C[3], almost twice the rate of the global average[4]. The resultant permafrost thaw leads to soil active layer deepening[5, 6], changes in surface vegetation composition[7, 8], altered carbon accumulation[2, 9] and shifts in microbial communities that degrade or transform OC[10-12]. Ultimately, permafrost peatlands are shifting from a carbon sink to a source of greenhouse gases (GHG)[1, 13, 14]. What controls how fast and to which extent this will occur is currently intensively studied.

One parameter relevant for controlling GHG emissions in permafrost environments could be protection of carbon by Fe minerals. Fe-OC associations regulate long-term global preservation of natural organic matter in soils and sediments and in the active layer underlain by intact permafrost and in partially-thawed soils[15, 16]. With permafrost thaw, this so-called rusty carbon sink[17] is lost and the mineral-bound OC is mobilized by reductive dissolution of Fe(III) minerals promoted by Fe(III)-reducing bacteria under water-logged and O_2 limited conditions[15]. The resulting dissolved OC (DOC) can then be further metabolized and can lead to GHG emissions along the permafrost thaw gradient[18].

However, permafrost peatlands not only experience long-term thaw, but also seasonal changes in freeze-thaw cycles[19], air temperature[20], sunlight[21] and precipitation[20]. With seasonal shifts in runoff and soil moisture[20], soils could drain and (re-)flood[22]. Redox conditions, which are controlled by the presence of electron acceptors such as O_2, fluctuate between oxic (oxygen-rich, drained) and anoxic (oxygen-depleted, flooded), where alternative electron acceptors (e.g., Fe(III), NO_3^-, SO_4^{2-}, CO_2) are converted to reduced species (e.g. Fe(II), NO_2^-/N_2, H_2S, CH_4).

Hence, these seasonal redox changes either promote or suppress Fe(III) reduction and Fe(II) oxidation, in turn influencing carbon mineralization and ultimately, GHG emissions[23-25]. To date, it remains unknown if the rusty carbon sink in permafrost peatlands is stable or continuously recycled by Fe(III) reduction and Fe(II) oxidation during seasonal redox fluctuations.

To capture the spatial and temporal dynamics of the rusty carbon sink over the thawed summer season from July to September, we exposed sand coated with synthetic Fe(III) oxyhydroxide minerals, ferrihydrite (FH; simplified formula of $Fe(OH)_3$), in the active layer in three thaw stages at a Swedish peatland (Stordalen mire, Abisko) in early (July) and late summer (July-September). The thaw stages in which the FH-coated sand was exposed in the active layer were (1) desiccating palsa underlain by permafrost, (2) partially-thawed bog, and (3) fully-thawed fen as previously defined[11, 18, 26, 27]. The objectives of this study were i) to quantify Fe(III) (oxyhydr)oxide formation, dissolution and transformation and ii) to quantify Fe-associated OC along the thaw gradient as redox conditions shift in the thawed summer season.

MATERIAL & METHODS

Field Site. Stordalen mire in the Abisko region of northern Sweden is a degrading permafrost peatland[28, 29]. Increasing mean annual air temperatures, exceeding the 0°C threshold, led to rapid warming of the Abisko region since the twentieth century[30] causing active layer deepening and an increase in surface wetness through thawing of permafrost[5]. As previously described[11, 15, 18], the mire consists of three distinct forms of degrading permafrost peatland: (1) palsa (intact permafrost), (2) ombrotrophic peatland or bog (partially-thawed) with *Sphagnum* spp., sedges and shrubs, and (3) minerotrophic peatland or fen (fully-thawed) with sedges, mainly *Eriophorum* spp.[26] (SI, Figure S1).

Exposure Experiment. To capture the spatial and temporal dynamics of the rusty carbon sink over the thawed summer season from July to September, we incubated sand coated with synthetic Fe(III) oxyhydroxides (here FH) in the Stordalen mire peatland. FH-coated sand was exposed for either two weeks in early summer (early July 2019) or two months in late summer (early July to September 2019) in the active layer of palsa, bog and fen along the previously described permafrost thaw gradient[15, 18] (for FH-coated sand synthesis and exposure bag preparation see SI, as well as Figures S1 and S2). For short-term exposure, three bags each were placed for 2 weeks (early summer) at three sites in each of the three thaw stages (9 bags per thaw stage in total; for exact positions see SI, Figure S1). For long-term exposure, three bags each were exposed for 2 months (late summer) at each of the three thaw stages (3 bags per thaw stage, 9 in total; SI, Figure S1). The first 10 cm of the soil layer were removed with a coring sleeve and the bags placed into the hole, which was then sealed again with the upper 10 cm soil. After the exposure times, the FH bags were carefully taken out of the soil, immediately frozen in liquid nitrogen and stored at -80°C until further analysis. Before soil extractions, further geochemical and microbial community analysis, the FH-coated sand that was incubated in different bags at the same thaw stage site (palsa, bog and fen) and collected at the same time

point was homogenized to have enough sample material to optimize the methods and to avoid limited sample volume for replicate analysis. The reported values represent the average and standard deviation of triplicate analysis of nine homogenized bags per thaw stage for the short-term exposure and three homogenized bags per thaw stage for the long-term exposure (SI, Figure S1). Unexposed FH-coated sand was used as a reference material.

Sequential Fe Extractions. Sequential Fe extractions were used to follow changes in solid-phase Fe transformation along the thaw gradient over the season. Anoxic Na-acetate solution (1 M, pH 5), followed by extractions with 0.5 M and 6 M HCl were used to successively dissolve Fe phases with increasing crystallinity[31]. Adsorbed Fe(II)[32, 33] and Fe in amorphous Fe sulfides[34] were extracted by the Na-acetate (referred to adsorbed/amorphous Fe). 0.5 M HCl was chosen to extract poorly crystalline Fe(III) (oxyhydr)oxides and remaining reduced Fe(II) species such as $FeCO_3$[35] or FeS (referred to as poorly crystalline Fe) and 6 M HCl to extract more crystalline, remaining Fe fractions, such as more crystalline Fe(III) (oxyhydr)oxides, poorly reactive sheet silicate Fe or FeS species[15, 31] (referred to as more crystalline Fe) from the Fe mineral coated sand (for exact extraction procedure see SI). Total Fe is calculated as the sum of Fe extracted by 1 M Na-acetate, 0.5 M and 6 M HCl.

Total Organic Carbon Analysis. To quantify TOC content of the sands after field exposure, triplicate samples of the homogenized samples (all bags per thaw stage and exposure time) were dried at 60°C until no further weight loss was observed. The samples were ground to fine powders and analyzed by a SoilTOC instrument (Elementar Analysensysteme GmbH, Germany).

Determination of OC bound to the Fe mineral surface. A sodium pyrophosphate extraction (pH 10) was used to remove loosely bound OC. This includes labile and microbial OC as well as OC in Fe-OC complexes and Fe-OC colloids[15, 36]. Sodium pyrophosphate solubilizes organic

matter (of labile OC and microbial origin), dissolves Fe from organic complexes, and promotes peptization and dispersion of Fe oxide colloids which makes it difficult to specify the source of extracted Fe and OC[37, 38] The same amounts of homogenized sand and extract were used as for the sequential Fe extraction, only the incubation time was extended to 16 h, as previously suggested[15, 36]. The Fe extracted by the sodium pyrophosphate extraction, representing colloidal/OM-chelated Fe, was negligible (0.00±0.00 to 0.18 mg sodium pyrophosphate extractable Fe per g sand) in comparison to the total Fe (1.02±0.09 to 5.59±0.46 mg Fe per g sand, 0.04 to 18.06% of the total Fe). The OC extracted by the sodium pyrophosphate extraction is implicated in complex association structures, such as colloids or aggregates, but not mineral-bound OC[36, 39]. Given i) that the bags consisted only of FH and quartz, and ii) that crystalline quartz such as that present in the bags has low potential for complexation with organic compounds[40], we assume that all of the carbon quantified via total organic carbon (TOC) of the FH coated sands after subtracting loosely bound OC (sodium pyrophosphate extractable OC) is strongly associated with the present Fe mineral surface (equation 1):

$$OC\ bound\ to\ Fe\ mineral\ surface = TOC - sodium\ pyrophosphate\ extractable\ OC$$

Geochemical Analyses. Extracts (supernatants) were analyzed in technical triplicates for Fe (extracted by sodium acetate, 0.5 M HCl or 6 M HCl or sodium pyrophosphate) and OC (extracted by sodium pyrophosphate)[15]. Extracts for Fe analysis were immediately stabilized under anoxic conditions in 1 M HCl dilutions. Fe(II) and Fe(tot) were determined by the spectrophotometric Ferrozine assay[41] within 24 h. DOC was quantified in triplicate with a TOC analyzer (High TOC II, Elementar, Elementar Analysensysteme GmbH, Germany). Inorganic carbon was removed by acidifying the samples with 2 M HCl prior to analysis.

Scanning Electron Microscopy (SEM) and Energy Dispersive X-Ray Analysis (EDS) was conducted as described in the SI.

Microbial Community Analysis. Total DNA was extracted as described previously[42]. Briefly, the PowerSoil® RNA and DNA isolation kit was used to extract DNA in triplicates from homogenized bags per thaw stage and exposure time with the following modifications: 2 g of sand was used from each bag; beat-beating was conducted for 10 mins and centrifugation was at maximum speed (7,000g) at 4°C. During extractions, incubation time was extended to 1.5 h at -20°C (for details see SI). Library preparation steps and sequencing were performed by Microsynth AG (Switzerland) as detailed in the SI. Quality control, reconstruction of 16S rRNA gene sequences and taxonomic annotation was performed with nf-core/ampliseq v1.1.2[43, 44] as outlined in the SI.

Isolation of Fe(III)-reducing bacteria was performed with anoxic synthetic fresh water media (as previously described[15]) using a dilution to extinction approach (for further information see SI).

Seasonal Monitoring. To capture seasonal fluctuations in weather and soil geochemical conditions, context data such as precipitation, air temperature, soil moisture and soil temperature were analyzed. Precipitation and air temperature data were provided by the Abisko Observatory. Soil moisture and soil temperature data were provided by Integrated Carbon Observation System (ICOS) Sweden Abisko – Stordalen[45]. Redox potentials in the palsa, bog, and fen were continuously monitored with five redox potential probes (PaleoTerra). Two probes were positioned in both the bog and fen and one was positioned in the palsa. Each redox probe had platinum sensors positioned at 6, 8 and 10 cm depth below the ground surface (for details see SI).

RESULTS & DISCUSSION

Seasonal fluctuations drive redox shifts in thawing permafrost peatlands. Snow melt began in the second half of April in 2019 (air temperatures above 0°C, Figure 1) and lasted around one month. As previously shown, the melt water results in highest annual runoff (up to 75% of the total annual runoff)[20], which was reflected in our own data set by the volumetric soil water content (VSWC). VSWC was highest in the intact palsa (51%) between the end of March and the beginning of April (Figure 1), presumably resulting in increasing runoff into the partially-thawed bog[46]. In early summer, semi-wet bog soils were weakly (+100 to +300 mV[47]) to moderately (-100 to +100 mV[47]) reduced from 6 to 10 cm depth (Figure 1 and SI, Figure S4). From the beginning of the thawed season (soil temperatures above 0°C in May/June), the air temperature increased to a maximum of 18.7°C, accompanied by a soil temperature increase to a maximum of 25.0°C in 2 cm soil depth at the end of July (Figure 1). Increasing evapotranspiration, together with decreasing runoff from intact palsa (VSW of 26%) and increasing active layer depth (30 to 70 cm)[20, 22, 26], led to soil drainage in the partially-thawed bog (Figure 1 and SI, Figure S4). Ultimately, a shift from weakly/moderately reduced to oxic conditions (redox potential above +300 mV) in late summer was observed (Figure 1 and SI, Figure S5).

Through the whole thaw season, the palsa remained relatively dry and oxic (SI, Figure S5), whereas the fen stayed water-logged (VSWC of 40%, Figure 1) and weakly to moderately reduced (SI, Figure S5), confirming previous studies[18, 48]. The annual average air temperature of +0.2°C slightly exceeded the 0°C threshold (above 0°C ice melts and permafrost thaws) supporting the overall warming trend since the early 20th century[30]. The summer of 2019 was dry: only 60 mm rain fell in June and July (Figure 1) compared to the long-term average of 81 mm (1913-2009)[20].

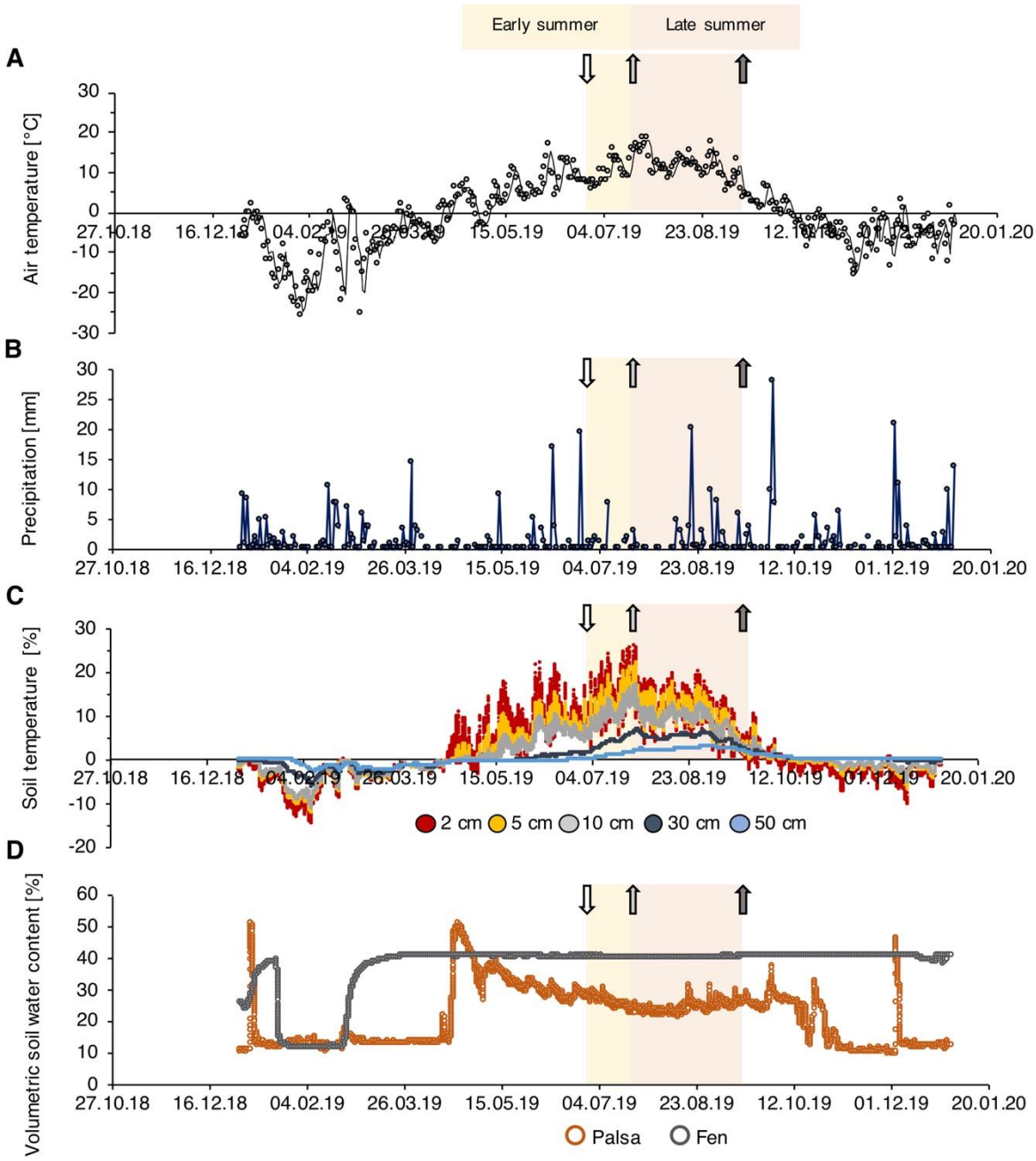

Figure 1. Seasonal fluctuations in weather and soil conditions for Abisko and Stordalen mire in the year 2019. (A) Air temperature [°C] and (B) precipitation [mm] were monitored by the Abisko Observatory. (C) Average soil temperature at Stordalen mire (average of the three thaw stages palsa, bog and fen) at 2 cm, 5 cm, 10 cm, 30 cm and 50 cm depth and (D) volumetric soil water content [%] in the upper 6 cm from the soil surface in palsa and fen were monitored by Integrated Carbon Observation System (ICOS) Sweden Abisko-Stordalen[45]. For thaw stage specific soil temperatures see SI, Figure S6. Early summer (yellow background)

marks the time period when the short-term ferrihydrite (FH) bags were exposed for 2 weeks and late summer (red background) the additional time period when the remaining FH bags were exposed (in total: 2 months). White arrow marks start of short and long-term exposure. Light grey arrow marks end of short-term exposure (exposed in early summer) and dark grey marks the end of the long-term exposure (exposed in early to late summer).

Fe(III) mineral formation and dissolution under changing redox conditions. In the active layer of the palsa underlain by intact permafrost, continuous oxic conditions promoted Fe(II) oxidation to Fe(III) phases through early to late summer, presumably from the influx and oxidation of dissolved Fe(II) from the surrounding soil. A 62.1 to 155.3% gain in solid Fe(III) (0.5 M HCl and 6 M HCl extractable) was observed in bags exposed in early to late summer (3.55±0.82 to 5.58±0.35 mg Fe(III) per g sand in comparison to 2.19±0.26 mg per g sand in the reference material). In the active layer of the partially-thawed bog, weakly to moderately reduced redox conditions in early summer favored Fe(III) (oxyhydr)oxide reduction which is indicated by Fe(III) mineral dissolution leading to a 52.5% loss of Fe (i.e. loss of 1.03±0.34 mg 0.5 M HCl extractable Fe(III) per g sand, Figure 2). However, a shift to predominantly oxic conditions in the bog in the late summer, caused by seasonal redox fluctuations, promoted net Fe(II) oxidation, indicated by a 33.3% gain in Fe(III) in the bags exposed until late summer relative to the reference material. The newly formed Fe phase was more crystalline, as indicated by a gain in 0.73±0.21 mg 6 M HCl extractable Fe per g sand in comparison to the reference material (that contained 1.01±0.14 mg 6 M HCl extractable Fe per g sand, probably due to aging over time) (Figure 2).

In the active layer of the fully-thawed fen, continuous weakly to moderately reducing conditions led to substantial Fe loss and slight Fe(II) accumulation through early to late summer. 50.4%

Fe(III) was lost from the solid phase (0.98±0.08 mg Fe(III) remaining) and 0.11±0.01 mg Fe(II) per g sand (1 M Na-acetate extractable) were formed during exposure.

The gain of poorly crystalline Fe in bags exposed in the active layer of intact palsa, attributed to Fe(II) oxidation under oxic conditions, supports previous observations showing highest amounts of Fe(III) (oxyhydr)oxides at the redox interface between shallow organic and deeper mineral horizons within the seasonally thawed active layer overlying intact permafrost[15, 49]. Fe(III) formation during late summer, as observed in bags exposed in the active layer of the partially-thawed bog, could explain the presence of reactive Fe(III) phases in bog soils: Patzner *et al.*[15] found that 7.5% of the total Fe (6M HCl extractable) in partially-thawed bog soils was reactive Fe(III) (i.e. sodium dithionite citrate extractable[50]). The newly formed, more crystalline Fe(III) phase in bags exposed in the bog until late summer could be explained by exposure of poorly crystalline Fe(III) oxyhydroxide minerals to microbially derived Fe(II) which can induce mineral recrystallization and transformation processes of Fe(III) oxyhydroxides towards thermodynamically more stable mineral phases[51]. Along the thaw gradient, aqueous Fe(II) in the porewater increased from 0.02±0.01 mM in the palsa to up to 1.6±0.3 mM in the fen[15] and the pH from 4.1 in the bog to 5.8 in the fen[18]. Fe(II)-catalyzed transformation of FH can result in either goethite (α-FeOOH), lepidocrocite (γ-FeOOH) or magnetite (Fe_3O_4) formation with only minor differences in pH, background ligands, and Fe(II):Fe(III) ratios impacting reaction kinetics and end-phase[51-55]. The presence of DOC in the partially thawed bog[15, 18] could also cause mineral transformation to less-crystalline FH and lepidocrocite through FH dissolution and then reprecipitation as Fe-OC co-precipitates[56]. Exposed FH on the sand grains could also trigger a so-called template effect: Chen and Thompson[57] observed goethite formation in various forest soils promoted by a template effect of pre-existing Fe(III) (oxyhydr)oxides. The non-extractable mineral phase (here: quartz) has only a minor effect on oxidation rates[57]. Further studies are needed to identify the newly formed Fe phases by, e.g. Mössbauer

spectroscopy or XRD analysis, which for this experimental setup was not possible due to the high background of quartz in the sand grains in comparison to the much lower Fe content.

Our incubation experiments provide a mechanistic explanation for the Fe(II) concentrations observed before in fen soil at Stordalen mire (Sweden)[15] and in other Arctic peat soils in Barrow (Alaska)[58]. Lipson *et al.*[59] estimated that net reduction of Fe(III) (oxyhydr)oxides coupled to oxidation and mineralization of OC contributes to 40-63% of ecosystem respiration depending on organic layer thickness and season. In the FH-exposed bags, Fe(III) reduction was most likely driven by Fe(III)-reducing bacteria such as *Geobacter* spp. We successfully isolated Fe(III)-reducing bacteria from the FH-coated sand in bags exposed in the fen with a 16S rRNA gene sequence that shares 98% identity to *Geobacter* spp. In addition, *Geobacter* spp. comprised 0.45±0.01% relative abundance in 16S rRNA gene amplicon sequencing of the whole microbial community associated with exposed sand in the fully-thawed fen until late summer (see SI, Figure S7 and S8).

We observed incomplete Fe(III) reduction and dissolution from bags exposed in the bog and fen, resulting in 52.6% loss of the initial Fe(III) in the bog in early summer and 50.4% loss of the initial Fe(III) in the fen through the whole summer. The remaining Fe(III) phase in our exposure experiments might explain the presence of small quantities of reactive Fe(III) phases (2.64±0.03 mg Fe per g soil) at the redox boundary between organic and mineral horizon in the fully-thawed fen, suggesting a minor but persistent Fe fraction remaining in soils even with complete permafrost thaw[15]. This incomplete Fe(III) reduction and dissolution could have a number of explanations: (1) The Teflon bag itself may slow Fe(III) reduction rates probably due to slightly limited access for bacteria and hydrophobicity of the Teflon: in Teflon packed FH-coated sands, Fe(III) reduction rates were slightly lower than in unpacked FH-coated sand (SI, Figure S9). (2) Exposed FH-coated sand could have a lower susceptibility to reductive dissolution compared to aluminum-silicate-FH coprecipitates[60] which are typically present in

soils. (3) Remaining Fe(III) minerals are less accessible for microbial Fe(III) reduction due to formation of Fe(II)-surface coatings which lower the reducibility of Fe minerals[39]. (4) The remaining Fe(III) phase could also be sustained by present Fe(II)-oxidizing bacteria such as *Gallionella* spp. and *Sideroxydans* spp. (SI, Figure S7 and S8), although this seems to be unlikely due to very low dissolved O_2 concentrations (0.15±0.04 µM in partially-thawed bog and 0.02±0.01 µM in fully-thawed fen in early summer, i.e. mid-July[48]).

The remaining Fe(III) phase could also be explained by net oxidation of Fe(II) even under reduced conditions. Previously, Lipson *et al.*[59] observed net oxidation of Fe(II) in the active layer of reduced permafrost soils for which several hypotheses are suggested: (1) Fe(II) oxidation by O_2 or by microaerophilic Fe(II)-oxidizers could be driven by transport of oxygen to deeper layers by plant roots[61], such as *Eriophorum* spp. at Stordalen mire, (2) high concentration of dissolved Fe in these soils (1.6±0.3 mM aqueous Fe^{2+} [15]) that might circulate throughout the soil profile, becoming oxidized to Fe(III) abiotically by O_2 or by microaerophilic Fe(II)-oxidizers at the surface and diffusing to lower layers, (3) oxidation of Fe(II) under anoxic conditions e.g. by microbes coupled to nitrate reduction, abiotically by reactive N-species (e.g. nitrite), perchlorate reduction, by phototrophic Fe(II)-oxidizers or radicals formed by light[62, 63]; or (4) direct flow of e^- through conductive soil components such as metal (e.g. Fe) ions in the porewater and electric double layer of colloidal surfaces of organic matter and metal ions (highly abundant in peat soils[64]) that can couple anoxic processes at depth to oxic processes at the surface[65]. One such conductivity component could even be caused by the presence of cable bacteria that link the oxidation of Fe(II) in anoxic layers to the reduction of O_2 at the surface[42] and/or *Geobacter* spp. (SI, Figure S7 and S8) which produces conductive biofilms, pilin nanofilaments (known as microbial nanowires) and nanoparticulate Fe (oxyhydr)oxides[66, 67] that form conductive networks over centimeter scales with Fe(III)-reducing microbial cells[68] and humic substances that can shuttle electrons to Fe(III) (oxyhydr)oxides[69].

The exposure experiments reveal the presence of the rusty carbon sink in intact permafrost soils, which is lost with complete permafrost thaw[15]. Our new findings suggest a more dynamic microbial iron cycle in the intermediate, partially-thawed bog, under seasonal fluctuations in the thawed active layer, either promoting or suppressing Fe(II) oxidation and thus Fe(III) mineral formation.

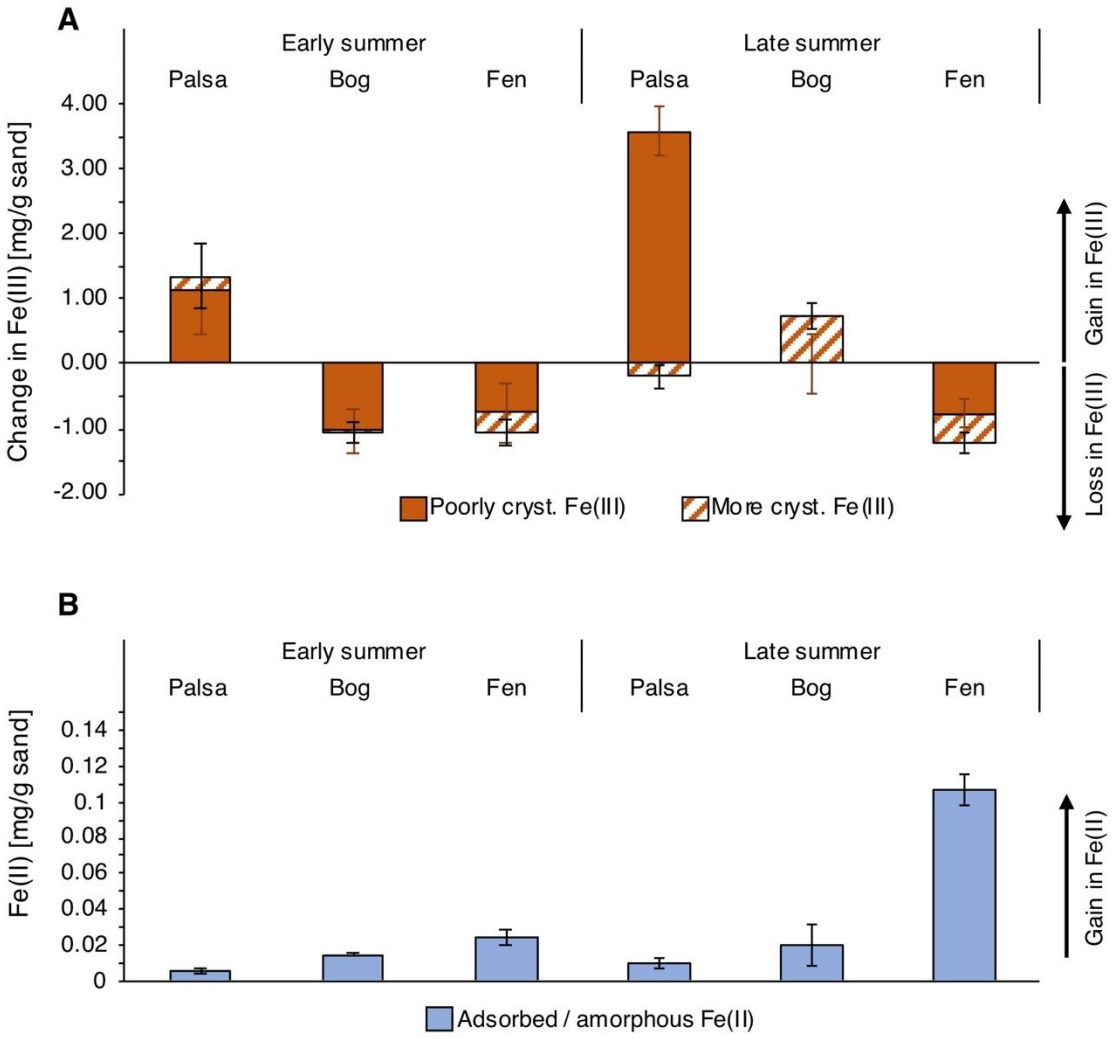

Figure 2. Gain and loss of solid-phase iron (Fe) along a thaw gradient in early (2 weeks exposure) and till late summer (2 months exposure). (A) Gain and loss in poorly crystalline Fe(III) (0.5 M HCl extractable) and more crystalline Fe(III) (6 M HCl extractable). Values are normalized to the reference material (unexposed ferrihydrite (FH)-coated sand with 2.19±0.26 mg total Fe per g sand), which was transported to the field but then stored at room temperature

until the end of the experiment. The reference material included a more crystalline Fe phase (1.01±0.14 mg only 6 M HCl extractable per g sand), probably due to aging over time. Positive values indicate a net gain in Fe and negative values indicate a net loss in Fe in comparison to the reference material. (B) Adsorbed/amorphous Fe(II) (1 M Na-acetate extractable). No Fe(III) was detected in the 1 M Na-acetate extracts. Reported values for the early summer period are the average and error bars are the combined standard deviation of triplicate analysis, normalized to the reference material, of nine homogenized bags, exposed at each thaw stage (palsa, bog and fen). Reported values for the late summer period are the average and error bars are the combined standard deviation of triplicate analysis, normalized to the reference material, of homogenized bags, exposed at each thaw stage (palsa, bog and fen).

Carbon sequestration by Fe mineral phases under changing redox conditions in thawing permafrost peatlands. In the active layer of palsa, almost no OC was associated with the Fe mineral phases after exposed in the early summer (0.05±0.07 mg OC per g sand) or exposed till the late summer (0.08±0.04 mg OC per g sand) (Figure 3). In early summer, almost no OC associated with the Fe mineral surface was observed in the bags exposed in the partially-thawed bog (0.02±0.02 mg OC per g sand) and fully-thawed fen areas (0.06±0.03 mg OC per g sand) along the thaw gradient, probably due to the overall loss of Fe caused by mineral dissolution. Carbon sequestered by Fe minerals on the sand grains was only observed in the active layer of the bog (0.82±0.05 mg OC per g sand) and in the fen (0.61±0.04 mg OC per g sand) at the end of the summer (Figure 3). This indicates strong associations of Fe with OC. OC/Fe (wt:wt) ratios were 0.28 in the bog and 0.73 in the fen at the end of the summer (see Table S1). These OC/Fe (wt:wt) ratios suggest co-precipitation with and/or chelation of metal (Fe) ions by organic compounds which can generate OC/Fe associates with C/Fe ratios (wt:wt) above 0.22[16,

[70-72]. Microscopic images of Fe-OC associations on the sand grain surface could indicate such co-precipitates of OC and Fe (Figure 4; SI Figure S10-S12).

It should be noted that exposed FH-coated sands cannot only capture the mobile phase of OC (i.e., DOC) in the porewater, but also particles smaller than 0.55 mm diameter, which is the size of the holes in the Teflon bags and thus would include particulate organic carbon and microbes. Along the thaw gradient, DOC increases from 19.7±0.8 mg/L in the palsa to 102.1±14.1 mg/L in the fen areas[15] and biomass increases with 2.6 times more microbial cells per gram of soil found in fully-thawed fen relative to palsa and bog[11]. The increasing microbial biomass along the thaw gradient may explain highest sodium pyrophosphate extractable OC of bags after long-term exposure in bog (34.13% of TOC) and fen (38.12% of TOC) (SI, Figure S3) and why our DNA extraction was only successful for bags exposed in fen till late summer (SI, Figures S7 and S8).

Previously, it was shown that OC associated with reactive Fe minerals was higher in intact palsa soils than in other soils (bog and fen) along a permafrost thaw gradient[15], whereas here in our field exposure experiments, Fe exposed in intact palsa soils did not sequester any OC. Dissolved Fe^{2+} in soils migrates upwards to the redox interface where it is oxidized to form Fe(III) (oxyhdyr)oxides or organic-bound Fe(III)[49]. This process leads to the observed increase of Fe in bags exposed in intact palsa soils, which we attribute primarily to Fe(III) (oxyhydr)oxide formation given the low abundance of pyrophosphate-extractable Fe (SI, Figure S3). DOC, however, is more dynamic as Fe as it might be metabolized and transformed to CO_2 and CH_4 prior to reaching the exposed FH we experimentally incubated in the active layer underlain by intact permafrost. Chen *et al.*[24] found dissolved organic matter (DOM) and soil organic matter (SOM) protection by Fe only under static oxic conditions when Fe^{2+} and DOC were both present. The exclusive presence of Fe^{2+} resulted in an increasing abiotic OC mineralization by

8% following oxidation to Fe(III)[24]. Abiotic oxidation of dissolved Fe^{2+} by O_2 produces hydroxyl radicals that are known to degrade organic matter to low molecular weight organic molecules and CO_2[73, 74]. Thus, the absence of DOC, due to its potential high bioavailability[75], as well as the radical formation following abiotic oxidation of dissolved Fe^{2+} by O_2 could explain the absence of OC associated with the exposed FH in the active layer of the palsa soils. Highest carbon sequestration in these exposure experiments occurred after Fe(II) oxidation and Fe(III) mineral formation in bags exposed in the active layer of the partially-thawed bog until late summer and could explain previous observations that highest percentages of reactive Fe-bound OC were found in bog soils along the thaw gradient after palsa collapse (39.4% of TOC was reactive Fe-associated at the redox boundary between organic and mineral horizon)[15]. However, our data shows that the rusty carbon sink in the active layer of the partially-thawed bog soils in permafrost peatlands is not stable over the thawed summer, but is continuously recycled by Fe(III) reduction and Fe(II) oxidation resulting in a shift from carbon source, shown by the lack of Fe-sequestered OC in early summer, towards a rusty carbon sink, shown by the presence of Fe-sequestered OC in late summer in the partially-thawed bog.

The sequestration of OC associated with the Fe mineral surface after mineral dissolution occurred are seen in the bags exposed in the fully-thawed fen until late summer. The Fe(III) oxides remaining in these bags by late summer seem resistant to mineral reduction and dissolution and can capture OC from the surrounding porewater. The presence of remaining Fe(III) oxides in the exposed FH bags after mineral reduction and dissolution could explain previous observations of small quantities of Fe(III)-OM (determined via extended X-ray absorption fine structure (EXAFS) and Fe(III)-citrate as reference probes) in fully-thawed fen soils[15]. However, it remains unclear, why, after mineral dissolution occurred, the Fe(III) mineral phases didn't sequester small amounts of OC in the bags in the partially-thawed bog and fully-thawed fen after early summer exposure. Explanations could be differences in the mineralogy

of the remaining Fe(III) phase or Fe(II)-OC coatings on the sand grains surface in the fully-thawed fen, which is supported by the fact that highest solid Fe(II) was observed in bags in fully-thawed fen after late summer exposure. In fen soils, no reactive Fe-associated OC was determined[15].

Our data indicates different carbon sequestration mechanisms by Fe (oxyhydr)oxides in the active layer over summer along the permafrost thaw gradient and illustrates that soils shift from being a carbon dioxide source (via microbially mediated reductive Fe(III) mineral dissolution coupled to OC mineralization) in early summer to a rusty carbon sink (via formation of Fe (oxyhydr)oxide minerals and sequestration of associated OC either fixed by microbes living on the particles and/or trapped from DOC) in late summer in the partially-thawed bog. Thus, the rusty carbon sink strongly depends on seasonal fluctuations in runoff, soil moisture and ultimately, redox conditions.

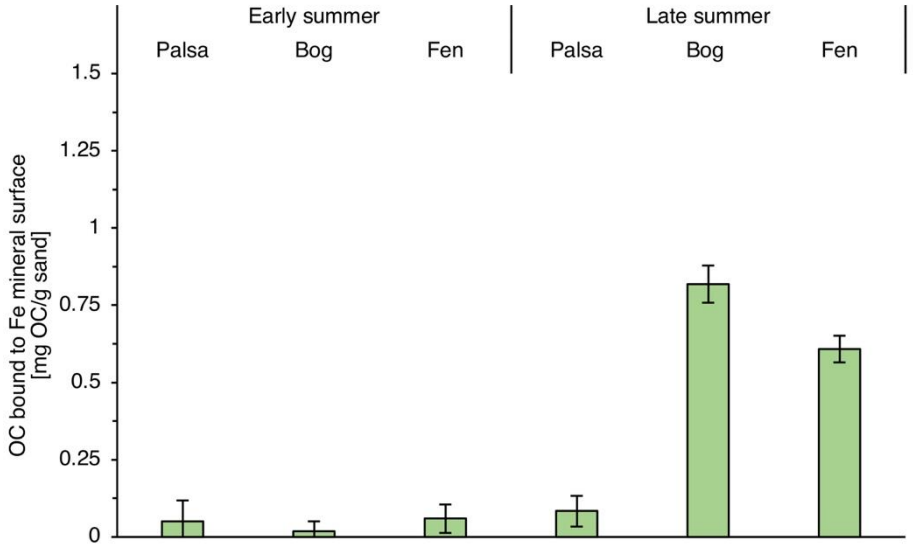

Figure 3. Organic carbon (OC) bound to iron (Fe) mineral phases along the thaw gradient in early (2 weeks exposure) and until late summer (2 months exposure). Reported values represent the total OC control-corrected by subtracting loosely bound OC (sodium

pyrophosphate extractable OC). Error bars represent the combined standard deviation of total OC and sodium pyrophosphate extractable OC.

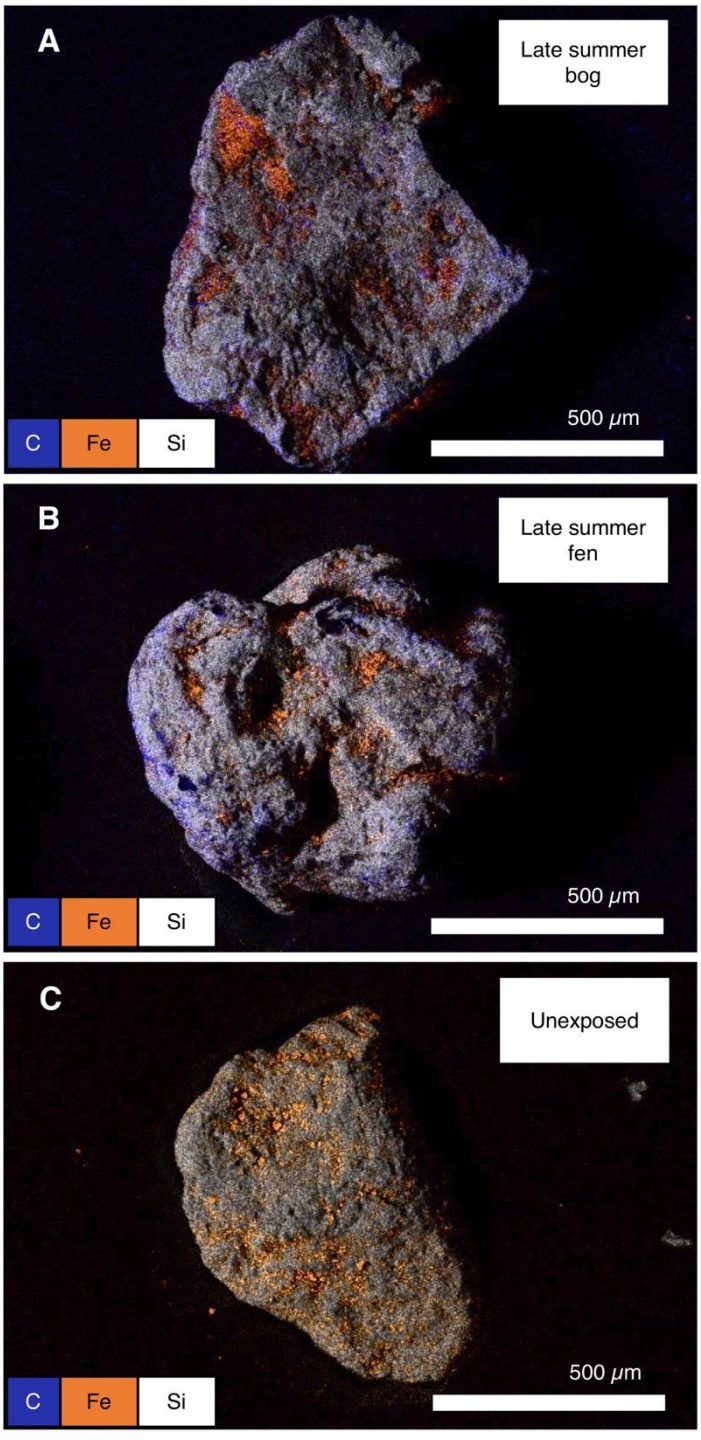

Figure 4. EDS derived chemical distribution maps of iron (Fe)-organic carbon (OC) associations on ferrihydrite (FH)-coated sand grains incubated in the partially-thawed

bog (A) and in fully-thawed fen (B) after late summer exposure (for 2 months) in comparison to the reference material (unexposed FH-coated sand) (C). Results shown are representatives and replicate analysis is reported in the Supporting Information (SI, Figures S11 and S12).

Environmental Implications. Permafrost environments experience drastic changes caused by global warming[13]. Rising temperatures in the Arctic[76] trigger increasing permafrost temperatures[77] and ultimately an increase in the thickness and variability of the active layer[78]. Multiple evidence exists that the Arctic hydrological cycle is intensifying because of warming[79], leading to a rise in all fluxes including precipitation, runoff and evapotranspiration[80]. These changes ultimately drive rapid shifts in water levels and redox conditions from flooded and more reduced to drained and oxic permafrost-affected soils[81]. The present study demonstrates that iron cycling in thawing permafrost peatlands correlates with redox conditions and that shifts in redox conditions resulted in either Fe(II) oxidation and Fe(III) mineral formation, sequestering OC, or leading to Fe(III) reduction, resulting in OC release. Iron cycling between Fe(II) and Fe(III) depending on shifts in redox conditions driven by seasonal fluctuations in runoff and soil moisture was also shown in a drained thaw lake basin on the Arctic coastal plain[59]. Thus, the seasonality of the rusty carbon sink in permafrost environments can strongly drive GHG emissions. On the one hand, Fe(III) reduction leads to direct CO_2 emissions since it is coupled to oxidation and mineralization of organic matter[59, 63]. Additionally, the released previously Fe-associated OC becomes more accessible to decomposers such as e.g. fermenters[11]. Fe(III) reduction can also inhibit methanogenesis by being more thermodynamically favorable[84]. McCalley *et al.*[10] found seasonal variations in CH_4 fluxes and their ^{13}C content in partially-thawed bog and fully-thawed fen at Stordalen mire, which could be partly driven by the use of Fe(III) in microbial metabolisms. On the other hand,

stable and newly formed Fe(III) minerals can sequester carbon and protect it from microbial consumption[85, 86], thus suppressing GHG emissions. Lee *et al.*[82] observed nearly 20 times lower carbon release on a per gram soil basis via aerobic respiration in incubation experiments with permafrost-affected mineral soils in comparison to organic soils. This lower carbon release in mineral soils could be caused by mineral OC sequestration. Adhikari *et al.*[83] demonstrated nearly 30% lower aerobic respiration of ferrihydrite-sorbed glucose and ferrihydrite-sorbed formic acid as compared to free glucose and formic acid. Future studies should assess the extent of GHG emissions caused by formation, transformation and destruction of Fe(III) minerals under fluctuating redox conditions in thawing permafrost environments.

Recently, Coward *et al.*[39] suggested that Fe-OC associations might be protected by surface coatings or by being embedded in a composite aggregate strucutre[87]. Thus, future *in situ* experiments should be conducted with a more complex matrix such as Fe-OC co-precipitates or biogenically derived Fe(III) (oxyhydr)oxides and in the presence of other important ions in soils (e.g. Si and Al).

ASSOCIATED CONTENT:

This manuscript is accompanied by Supporting Information, an extra document containing twenty pages and in total eleven figures.

DATA AVAILABILITY:

All data available in the supplementary information.

AUTHOR INFORMATION:

Corresponding author:

*e-mail: casey.bryce@bristol.ac.uk

Author Contributions:

The original hypothesis was formulated by M.S.P, C.B and A.K. M.S.P, C.B and A.K designed the project, interpreted the data and wrote the manuscript. M.S.P and E.L collected the samples. M.S.P gathered the data presented in the main text. Supporting information was collected by N.K, M.B and C.S. E.H and L.K.-C contributed to the data analysis and interpretation. S.F and M.S.P performed the SEM and EDS analysis. D.S processed the amplicon sequencing data and, together with S.K, helped with interpretation of the microbial community results. All authors contributed to the preparation of the manuscript and have given approval to the final version of the manuscript.

Notes:

The authors declare no competing interests.

ACKNOWLEDGEMENTS:

The authors would like to acknowledge the Swedish Polar Research Secretariat and SITES for the support of the work done at the Abisko Scientific Research Station, as well as ICOS Sweden (Swedish Research Council: 2019-00205) for their support during sampling missions and providing the context data (precipitation, air temperature, soil temperature, soil moisture), with special thanks to Annika Kristoffersson and Jutta Holst. thank the We thank Merritt Logan (Colorado State University, Fort Collins, Colorado) and Hanna Joss (University Tuebingen, Germany) for assistance in the field and for carbon analyzes. This work was supported by the University of Tuebingen (Programme for the Promotion of Junior Researchers award to Casey Bryce) and by the German Academic Scholar Foundation (scholarship to Monique S. Patzner). A.K acknowledges infrastructural support by the Deutsche Forschungsgemeinschaft (DFG, German Research Foundation) under Germany's Excellence Strategy, cluster of Excellence EXC2124, project ID 390838134. We also thank the German Research Foundation DFG (INST 37/1027-1 FUGG) for financial support provided for the acquisition of the cryogenic focused ion beam scanning electron microscope.

REFERENCES:

1. Schuur, E. A. G.; McGuire, A. D.; Schadel, C.; Grosse, G.; Harden, J. W.; Hayes, D. J.; Hugelius, G.; Koven, C. D.; Kuhry, P.; Lawrence, D. M.; Natali, S. M.; Olefeldt, D.; Romanovsky, V. E.; Schaefer, K.; Turetsky, M. R.; Treat, C. C.; Vonk, J. E. Climate change and the permafrost carbon feedback. *Nature* **2015,** *520*, (7546), 171-179.
2. McGuire, A. D.; Anderson, L. G.; Christensen, T. R.; Dallimore, S.; Guo, L. D.; Hayes, D. J.; Heimann, M.; Lorenson, T. D.; Macdonald, R. W.; Roulet, N. Sensitivity of the carbon cycle in the Arctic to climate change. *Ecol Monogr* **2009,** *79*, (4), 523-555.
3. Christensen, J. H., Kanikicharla, K.K. *et al*. Climate phenomena and their relevance for future regional climate change. Climate Change 2013 the Physical Science Basis: Working Group I Contribution to the Fifth Assessment Report of the Intergovernmental Panel on Climate Change. *Cambridge University Press* **2013**, 1217-1308.

4. IPCC, Climate change 2007: the physical science basis," in Contribution of Working Group I to the Fourth Assessment Report of the Intergovernmental Panel on Climate Change, eds S. Solomon, D. Qin, M. Manning, Z. Chen, M. Marquis, K. B. Averyt, M. Tignor and H. L. Miller (Cambridge, New York, NY: Cambridge University Press) **2007**.

5. Swindles, G. T.; Morris, P. J.; Mullan, D.; Watson, E. J.; Turner, T. E.; Roland, T. P.; Amesbury, M. J.; Kokfelt, U.; Schoning, K.; Pratte, S.; Gallego-Sala, A.; Charman, D. J.; Sanderson, N.; Garneau, M.; Carrivick, J. L.; Woulds, C.; Holden, J.; Parry, L.; Galloway, J. M. The long-term fate of permafrost peatlands under rapid climate warming. *Sci Rep* **2015,** *5*, 17951.
6. Hugelius, G.; Loisel, J.; Chadburn, S.; Jackson, R. B.; Jones, M.; MacDonald, G.; Marushchak, M.; Olefeldt, D.; Packalen, M.; Siewert, M. B.; Treat, C.; Turetsky, M.; Voigt, C.; Yu, Z. C. Large stocks of peatland carbon and nitrogen are vulnerable to permafrost thaw. *P Natl Acad Sci USA* **2020,** *117*, (34), 20438-20446.
7. Malmer, N.; Johansson, T.; Olsrud, M.; Christensen, T. R., Vegetation, climatic changes and net carbon sequestration in a North-Scandinavian subarctic mire over 30 years. *Global Change Biol* **2005,** *11*, (11), 1895-1909.
8. Xiao-Ying, J., Hui-Jun, J., Iwahana, G., Marchenko, S.S., Dong-Liang, L., Xiao-Ying, L., Si-Hai, L. Impacts of climate-induced permafrost degradation on vegetation: A review. . *Advances in Climate Change Research* **2020**, *1*, (1), 29-47.
9. Olid, C.; Klaminder, J.; Monteux, S.; Johansson, M.; Dorrepaal, E. Decade of experimental permafrost thaw reduces turnover of young carbon and increases losses of old carbon, without affecting the net carbon balance. *Global Change Biol* **2020,** *26*, (10), 5886-5898.
10. McCalley, C. K.; Woodcroft, B. J.; Hodgkins, S. B.; Wehr, R. A.; Kim, E. H.; Mondav, R.; Crill, P. M.; Chanton, J. P.; Rich, V. I.; Tyson, G. W.; Saleska, S. R. Methane dynamics regulated by microbial community response to permafrost thaw. *Nature* **2014,** *514*, (7523), 478-481.
11. 11. Woodcroft, B. J.; Singelton, C. M; Boyd, J. A.; Evans, P. N.; Emerson, J. B.; Zayed, A. A. F.; Hoelzle, R. D.; Lamberton, T. O.; McCalley, C. K.; Hodgkins, S. B.; Wilson, R. M.; Purvine, S. O.; Nicora, C. D.; Li, C.; Frolking, S.; Chanton, J. P.; Crill, P. M.; Saleska, S. R.; Rich, V. I.; Tyson, G. W. Genome-centric view of carbon processing in thawing permafrost. *Nature* **2018**, 560, 49-54.
12. Mackelprang, R.; Waldrop, M. P.; DeAngelis, K. M.; David, M. M.; Chavarria, K. L.; Blazewicz, S. J.; Rubin, E. M.; Jansson, J. K. Metagenomic analysis of a permafrost microbial community reveals a rapid response to thaw. *Nature* **2011,** *480*, (7377), 368-U120.

13. Turetsky, M. R.; Abbott, B. W.; Jones, M. C.; Anthony, K. W.; Olefeldt, D.; Schuur, E. A .G.; Grosse, G.; Kuhry, P.; Hugelius, G.; Koven C.; Lawrence, D. M.; Gibson, C.; Sannel, A. B .K.; McGuire, A. D. Carbon release through abrupt permafrost thaw. *Nat Geosci* **2020,** *13*, 138-143.
14. Lundin, E. J.; Klaminder, J.; Giesler, R.; Persson, A.; Olefeldt, D.; Heliasz, M.; Christensen, T. R.; Karlsson, J. Is the subarctic landscape still a carbon sink? Evidence from a detailed catchment balance. *Geophys Res Lett* **2016,** *43*, (5), 1988-1995.
15. Patzner, M. S.; Mueller, C. W.; Malusova, M.; Baur, M.; Nikeleit, V.; Scholten, T.; Hoeschen, C.; Byrne, J. M.; Borch, T.; Kappler, A.; Bryce, C. Iron mineral dissolution releases iron and associated organic carbon during permafrost thaw. *Nat Commun* **2020**, *11,* 6329.
16. Mu, C. C.; Zhang, T. J.; Zhao, Q.; Guo, H.; Zhong, W.; Su, H.; Wu, Q. B., Soil organic carbon stabilization by iron in permafrost regions of the Qinghai-Tibet Plateau. *Geophys Res Lett* **2016,** *43*, (19), 10286-10294.
17. Eglinton, T. I., GEOCHEMISTRY A rusty carbon sink. *Nature* **2012,** *483*, (7388), 165-166.
18. Hodgkins, S. B.; Tfaily, M. M.; McCalley, C. K.; Logan, T. A.; Crill, P. M.; Saleska, S. R.; Rich, V. I.; Chanton, J. P., Changes in peat chemistry associated with permafrost thaw increase greenhouse gas production. *P Natl Acad Sci USA* **2014,** *111*, (16), 5819-5824.
19. Genxu, W., Hongchang, H., Taibin, L., The influence of freeze-thaw cycles of active layer on surface runoff in a permafrost watershed. *Journal of Hydrology* **2009,** *375*, (3-4), 438-449.
20. Olefeldt, D.; Roulet, N. T.; Bergeron, O.; Crill, P.; Bäckstrand, K.; Christensen, T. R. Net carbon accumulation of a high-latitude permafrost palsa mire similar to permafrost-free peatlands. *Geophys Res Lett* **2012,** *39*, (3), L03501.
21. Frolking, S. E.; Bubier, J. L.; Moore, T. R.; Ball, T.; Bellisario, L. M.; Bhardwaj, A.; Carroll, P.; Crill, P. M.; Lafleur, P. M.; McCaughey, J. H.; Roulet, N. T.; Suyker, A. E.; Verma, S. B.; Waddington, J. M.; Whiting, G. J. Relationship between ecosystem productivity and photosynthetically active radiation for northern peatlands. *Global Biogeochem Cy* **1998,** *12*, 115-126.
22. Bäckstrand, K.; Crill, P. M.; Jackowicz-Korczynski, M.; Mastepanov, M.; Christensen, T. R.; Bastviken, D. Annual carbon gas budget for a subarctic peatland, Northern Sweden. *Biogeosciences* **2010,** *7*, 95-108.
23. LaCroix, R. E.; Tfaily, M. M.; McCreight, M.; Jones, M. E.; Spokas, L.; Keiluweit, M. Shifting mineral and redox controls on carbon cycling in seasonally flooded mineral soils. *Biogeosciences* **2019,** *16*, (13), 2573-2589.
24. Chen, C.; Hall, S. J.; Coward, E.; Thompson, A. Iron-mediated organic matter decomposition in humid soils can counteract protection. *Nat Commun* **2020,** *11*, (1), 2255.
25. Gault, A. G.; Langley, S.; Ibrahim, A.; Renaud, R.; Takahashi, Y.; Boothman, C.; Lloyd, J. R.; Clark, I. D.; Ferris, F. G.; Fortin, D. Seasonal changes in mineralogy, geochemistry and microbial community of bacteriogenic iron oxides (BIOS) deposited in a circumneutral wetland. *Geomicrobiol J* **2012,** *29*, 161-172.
26. Johansson, T.; Malmer, N.; Crill, P. M.; Friborg, T.; Akerman, J. H.; Mastepanov, M.; Christensen, T. R. Decadal vegetation changes in a northern peatland, greenhouse gas fluxes and net radiative forcing. *Global Change Biol* **2006,** *12*, (12), 2352-2369.
27. Lupascu, M.; Wadham, J. L.; Hornibrook, E. R. C.; Pancost, R. D. Temperature Sensitivity of Methane Production in the Permafrost Active Layer at Stordalen, Sweden: a Comparison with Non-permafrost Northern Wetlands. *Arct Antarct Alp Res* **2012,** *44*, (4), 469-482.

28. Malmer, N. B. W. Peat Formation and Mass Balanec in Subarctic Ombrotophic Peatland around Abisko, Northern Scandinavia. . *Ecological Bulletins* **1996,** *45*, 79-92.
29. Kokfelt, U.; Rosen, P.; Schoning, K.; Christensen, T. R.; Forster, J.; Karlsson, J.; Reuss, N.; Rundgren, M.; Callaghan, T. V.; Jonasson, C.; Hammarlund, D. Ecosystem responses to increased precipitation and permafrost decay in subarctic Sweden inferred from peat and lake sediments. *Global Change Biol* **2009,** *15*, (7), 1652-1663.
30. Callaghan, T. V.; Bergholm, F.; Christensen, T. R.; Jonasson, C.; Kokfelt, U.; Johansson, M. A new climate era in the sub-Arctic: Accelerating climate changes and multiple impacts. *Geophys Res Lett* **2010,** *37*.
31. Lueder, U.; Maisch, M.; Laufer, K.; Jorgensen, B. B.; Kappler, A.; Schmidt, C. Influence of physical pertubation on Fe(II) supply in coastal marine sediments. *Environ Sci Technol* **2020,** *54*, 3209-3218.
32. Roden, E. E.; Zachara, J. M. Microbial reduction of crystalline iron(III) oxides: Influence of oxide surface area and potential for cell growth. *Environ Sci Technol* **1996,** *30*, 1618-1628.
33. Tessier, A.; Campbell, P. G.; Bisson, M. Sequential extraction procedure for the speciation of particulate trace metals. *Anal Chem* **1979** *51*, 844-851.
34. Shannon, R. D.; White, J. R. The selectivity of a squential extraction procedure for the determination of iron oxyhydroxides andiron sulfides in lake sediments. *Biogeochemistry* **1991,** *14*, 193-208.
35. Heron, G.; Crouzet, C.; Bourg, A. C.; Christensen, T. H. Speciation of Fe(II) and Fe(III) in contaminated aquifer sediments using chemical extraction techniques. *Environ Sci Technol* **1994,** *28*, 1698-1705.
36. Coward, E. K.; Thompson, A. T.; Plante, A. F. Iron-mediated mineralogical control of organic matter accumulation in tropical soils. *Geoderma* **2017,** *306*, 206-216.
37. Kaiser, K.; Zech, W. Defects in estimation of aluminum in humus complexes of podzolic soils by pyrophosphate extraction. *Soil Science* **1996,** *161*, (7), 452-458.
38. Schuppli, P. A.; Ross, G. J.; McKeague, J. A. The effective removal of suspended materials from pyrophosphate extracts of soils from tropical and temperate regions. *Soil Sci Soc Am J* **1983,** *47*, 1026-1032.
39. Coward, E. K.; Thompson, A.; Plante, A. F. Contrasting Fe speciation in two humid forest soils: Insight into organomineral associations in redox-active environments. *Geochim Cosmochim Ac* **2018,** *238*, 68-84.
40. Heckman, K.; V·zquez-Ortega, A.; Gao, X.; Chorover, J.; Rasmussen, C. Changes in water extractable organic matter during incubation of forest floor material in the presence of quartz, goethite and gibbsite surfaces. *Geochim Cosmochim Ac* **2011,** *75*, 4295-4309.
41. Stookey, L. L., Ferrozine - a New Spectrophotometric Reagent for Iron. *Anal Chem* **1970,** *42*, (7), 779-781.
42. Otte, J. M.; Harter, J.; Laufer, K.; Blackwell, N.; Straub, D.; Kappler, A.; Kleindienst, S. The distribution of active iron-cycling bacteria in marine and freshwater sediments is decoupled from geochemical gradients. *Method Enzymol* **2018,** *20*, (7), 2483-2499.
43. Ewels, P. A.; Peltzer, A.; Fillinger, S.; Patel, H.; Alneberg, J.; Wilm, A.; Garcia, M. U.; Di Tommaso, P.; Nahnsen, S. The nf-core framework for community-curated bioinformatics pipelines. *Nat. Biotechnol.* **2020,** *38*, (3), 276-278.
44. Straub, D.; Blackwell, N.; Langarica-Fuentes, A.; Peltzer, A.; Nahnsen, S.; Kleindienst, S. Interpretations of environmental microbial community studies are biased by the selected 16S rRNA (gene) amplicon sequencing pipeline. *Front Microbiol* **2020,** *11,* 550420.

45. Rinne, J., ICOS Sweden Ecosystem eco time series (ICOS Sweden), Abisko-Stordalen Palsa Bog, 2018-12-31–2019-12-31, https://hdl.handle.net/11676/s5oBzukX_FaXpHU___86QasO) **2021**.
46. Olefeldt, D.; Roulet, N. T. Effects of permafrost and hydrology on the composition and transport of dissolved organic carbon in a subarctic peatland complex. *J Geophys Res-Biogeo* **2012,** *117,* G01005.
47. Reddy, K. R., DeLaune, R.D., Biogeochemistry of wetlands: Science and applications. *CRC Press, Boca Raton, FL.* **2008**, ISBN 978-1-56670-678-0.
48. 46. Perryman, C. R.; McCalley, C. K.; Malhotra, A.; Florencia Fahnestock, M.; Kashi, N. N.; Bryce, J. G.; Giesler, R.; Varner, R. K. Thaw Transitions and Redox Conditions Drive Methane Oxidation in a Permafrost Peatland. *J Geophys Res-Biogeo* **2020**, *125*, (3), G005526.
49. Herndon, E. M.; Yang, Z. M.; Bargar, J.; Janot, N.; Regier, T.; Graham, D.; Wullschleger, S.; Gu, B. H.; Liang, L. Y. Geochemical drivers of organic matter decomposition in arctic tundra soils. *Biogeochemistry* **2015,** *126*, (3), 397-414.
50. Lalonde, K.; Mucci, A.; Ouellet, A.; Gelinas, Y. Preservation of organic matter in sediments promoted by iron. *Nature* **2012,** *483*, (7388), 198-200.
51. Hansel, C. M.; Benner, S. G.; Fendorf, S. Competing Fe(II)-induced mineralization pathaways of ferrihydrite. *Environ Sci Technol* **2005**, (39), 7147-7153.
52. Jones, A. M.; Collins, R. N.; Waite, T. D. Redox characterization of the Fe(II)-catalyzed transformation of ferrihydrite to goethite. *Geochim Cosmochim Ac* **2017**, (218), 257-272.
53. Pedersen, H. D., Postma, D., Jakobsen, R., Larsen, O. Fast transformation of iron oxhydroxides by catalytic action of aqueous Fe(II). *Geochim Cosmochim Ac* **2005**, (69), 3967-3977.
54. ThomasArrigo, L. K.; Mikutta, C.; Byrne, J.; Kappler, A.; Kretzschmar, R. Iron(II)-catalyzed iron atom exchange and mineralogical changes in iron-rich organic freshwater flocs: An iron isotope tracer study. *Environ Sci Technol* **2017**, (51), 6897-6907.
55. Yang, L.; Steefel, C.; Marcus, M. A.; Bargar, J. R. Kinetics of Fe(II)-catalyzed transformation of 6-line ferrihydrite under anaerobic flow conditions. *Environ Sci Technol* **2010**, (44), 5469-5475.
56. Chen, C.; Thompson, A. Ferrous iron oxidation under varying pO2 levels: The effects of Fe(III)/Al(III) oxide minerals and organic matter. *Environ Sci Technol* **2018,** *52*, 597-606.
57. Chen, C.; Thompson, A. The influence of native soil organic matter and minerals on ferroux iron oxidation *Geochim Cosmochim Ac* **2021**, (292), 254-270.
58. Lipson, D. A.; Jha, M.; Raab, T. K.; Oechel, W. C. Reduction of iron (III) and humic substances plays a major role in anaerobic respiration in an Arctic peat soil. *J Geophys Res-Biogeo* **2010,** *115*, G00I06.
59. Lipson, D. A., Raab, T.K., Goria, D., Zlamal, J. , The contribution of Fe(III) and humic acid reduction to ecosystem respiration in drained thaw lake basins of the Arcitc Coastal Plain. *Global Biogeochem Cy* **2013,** *27*, 399-409.
60. Masue-Slowey, Y.; Loeppert, R. H.; Fendorf, S. Alteration of ferrihydrite reductive dissolution and transformation by adsorbed As and structural Al: Implications for As retention. *Geochim Cosmochim Ac* **2011,** *75*, (3), 870-886.
61. Colmer, T. D. Long-distance transport of gaes in plants: A perspective on internal aeration and radial oxygen loss from roots. *Plant Cell Environ* **2003,** *26*, 17-36.
62. Weber, K. A.; Achenbach, L. A.; Coates, J. D. Microorganisms pumping iron: Anaerobic microbial iron oxdiation and reduction. *Nature Reviews Microbiology* **2006,** *4*, 752-764.

63. Kappler, A.; Bryce, C.; Mansor, M.; Lueder, U.; Byrne, J. M.; Swanner, E. An evolving view on biogeochemical cycling of iron. *Nat Rev Microbiol* **2021**.
64. Comas, X.; Slater, L. Low-frequency electrical properties of peat. *Water Resour. Res.* **2004,** *40*, W12414.
65. Nielsen, L. P.; Risgaard-Petersen, N.; Fossing, H.; Christensen, P. B.; Sayama, M. Electric currents couple spatially separated biogeochemical processes in marine sediment. *Nature* **2010,** *463*, 1071-1074.
66. 64. Malvankar, N. S.; Vargas, M.; Nevin, K. P.; Franks, A. E.; Leang, C.; Kim, B. C.; Inoue, K.; Mester, T.; Covalla, S. F.; Johnson, J. P.; Rotello, V. M.; Tuominen, M. T.; Lovley, D. R. Tunable metallic-like conducitivity in microbial nanowire networks. *Nat Biotechnol* **2011**, *6*, 573-579.
67. Regberg, A.; Singha, K.; Tien, M.; Picardal, F.; Zheng, Q.; Schieber, J.; Roden, E.; Brantley, S. L. Electrical conductivity as an indicator of iron reduction rates in abiotic and biotic systems. *Water Resour Res* **2011,** *47*, W04509.
68. Kato, S.; Nakamura, R.; Kai, F.; Watanbe, K.; Hashimoto, K. Respiratory interactions of soil bacteria with (semi)conductive iron-oxide minerals. *Method Enzymol* **2010,** *12*, 3114-3123.
69. Roden, E. E.; Kappler, A.; Bauer, I.; Jiang, J.; Paul, A.; Stoesser, R.; Konishi, H.; Xu, H. Extracellular electron transfer through microbial reduction of solid-phase humic substances. *Nat Geosci* **2010,** *3*, 417-421.
70. Wagai, R.; Mayer, L. M. Sorptive stabilization of organic matter in soils by hydrous iron oxides. *Geochim Cosmochim Ac* **2007,** *71*, (1), 25-35.
71. Kaiser, K.; Guggenberger, G. Sorptive stabilization of organic matter by microporous goethite: sorption into small pores vs. surface complexation. *Eur J Soil Sci* **2007,** *58*, (1), 45-59.
72. Herndon, E.; AlBashaireh, A.; Singer, D.; Chowdhury, T. R.; Gu, B. H.; Graham, D. Influence of iron redox cycling on organo-mineral associations in Arctic tundra soil. *Geochim Cosmochim Ac* **2017,** *207*, 210-231.
73. Hall, S. J.; Silver, W. L. Iron oxidation stimulates organic matter decomposition in humid tropical forest soils. *Global Change Biol* **2013,** *19*, (9), 2804-2813.
74. Trusiak, A.; Treibergs, L. A.; Kling, G. W.; Cory, R. M. The role of iron and reactive oxygen species in the production of CO2 in arctic soil waters. *Geochim Cosmochim Ac* **2018,** *224*, 80-95.
75. Patzner, M. S.; Logan, M.; McKenna, A.; Young, R. B.; Zhou, Z.; Joss, H.; Mueller, C. W.; Hoeschen, C.; Scholten, T.; Straub, D.; Kleindienst, S.; Borch, T.; Kappler, A.; Bryce, C. Microbial iron(III) reduction during palsa collapse promotes greenhouse gas emissions before complete permafrost thaw. *eartharxiv.org* (preprint, has not been peer reviewed*)* **2021**.
76. Stocker, T.; Qin, D.; Plattner, G.-K.; Tignor, M.; Allen, S.; Boschung, J.; *et al.* (Eds.), Climate Change 2013: The physical science basis. Contribution of Working Group I to the Fifth Assessment Report of the Intergovernmental Panel on Climate Change. Cambridge, UK; New York, NY: Cambridge University Press. **2013**.
77. Osterkamp, T. E., Characteristics of the recent warming of permafrost in Alaska. *J Geophys Res-Biogeo* **2007,** *F02S02*.
78. Romanovsky, V. E., Osterkamp, T.E., Effects of unfrozen water on heat and mass transport processes in the active layer and permafrost. *Permafrost Periglac* **2000,** *11*, (June), 219-239.
79. 77. Rawlins, M. A.; Steele, M.; Holland, M. M.; Adam, J. C.; Cherry, J. E.; Francis, J. A.; Groisman, P. Y.; Hinzman, L. D.; Huntington, T. G.; Kane, D. L.; Kimball, J. S.; Kwok, R.; Lammers, R. B.; Lee, C. M.; Lettenmaier, D. P.; McDonald, K. C.; Podest, E.; Pundsack, J. W.; Rudels, B.; Serreze, M. C.; Shiklomanov, A.; Skagseth, Ø.; Troy, T. J.;

729 Vörösmarty, C. J.; Wensnahan, M.; Wood, E. F.; Woodgate, R.; Yang, D.; Zhang, K.; Zhang,
730 T. Analysis of the Arctic system for freshwater cycle intensification: Observations and expec-
731 tations. *Journal of Climate* **2010**, *23*, 5715-5737.
732 80. Walvoord, M. A.; Kurylyk, B. L. Hydrologic impacts of thawing permafrost - a
733 review. *Vadose Zone Journal* **2016,** *15*, (6).
734 81. Elberling, B.; Christiansen, H. H.; Hansen, B. U., High nitrous oxide production from
735 thawing permafrost (vol 3, pg 332, 2010). *Nat Geosci* **2010,** *3*, (7), 506-506.
736 82. Lee, H.; Schuur, E. A. G.; Inglett, K. S.; Lavoie, M.; Chanton, J. P. The rate of
737 permafrost carbon release under aerobic and anaerobic conditions and its potential effects on
738 climate. *Global Change Biol* **2012,** *18*, 515-527.
739 83. Adhikari, D.; Dunham-Cheatham, S. M.; Wordofa, D. N.; Verburg, P.; Poulson, S. R.;
740 Yang, Y. Aerobic respiration of mineral-bound organic carbon in a soil. *Science of the Total*
741 *Environment* **2019,** *651*, 1253-1260.
742 84. Van Bodegom, P. M.; Scholten, J. C. M.; Stams, A. J. M. Direct inhibition of
743 methanogenesis by ferric iron. *FEMS Microbiology Ecology* **2004**, *49*, 261-268.
744 85. Kleber, M.; Eusterhues, K.; Keiluweit, M.; Mikutta, C.; Mikutta, R.; Nico, P. S.
745 Mineral-Organic Associations: Formation, Properties, and Relevance in Soil Environments.
746 *Adv Agron* **2015,** *130*, 1-140.
747 86. Totsche, K. U.; Amelung, W.; Gerzabek, M. H.; Guggenberger, G.; Klumpp, E.;
748 Knief, C.; Lehndorff, E.; Mikutta, R.; Peth, S.; Prechtel, A.; Ray, N.; Kogel-Knabner, I.
749 Microaggregates in soils. *J Plant Nutr Soil Sc* **2018,** *181*, (1), 104-136.
750 87. Asano, M.; Wagai, R. Evidence of aggregate hierarchy at micro- to submicron scales
751 in an allophanic Andisol. *Geoderma* **2014,** *216*, 62-74.

752

753 Seasonal fluctuations of the rusty carbon sink in thawing permafrost peatlands

754

755

*Monique S. Patzner[1], Nora Kainz[1], Erik Lundin[2], Maximilian Barczok[3], Chelsea Smith[4], Elizabeth Herndon[5], Lauren Kinsman-Costello[4], Stefan Fischer[6], Daniel Straub[7,8], Sara Kleindienst[7], Andreas Kappler[1,9] & Casey Bryce[10]**

[1]*Geomicrobiology, Center for Applied Geosciences, University of Tuebingen, Germany.*

[2]*Swedish Polar Research Secretariat, Abisko Scientific Research Station, Sweden.*

[3]*Department of Geology, Kent State University, US.*

[4]*Department of Biological Sciences, Kent State University, US.*

[5]*Environmental Sciences Division, Oak Ridge National Laboratory, 1 Bethel Valley Rd, Oak Ridge, TN 37830, US.*

[6]*Tuebingen Structural Microscopy Core Facility, Center for Applied Geosciences, University Tuebingen, Germany.*

[7]*Microbial Ecology, Center for Applied Geosciences, University Tuebingen, Germany.*

[8]*Quantitative Biology Center (QBiC), University Tuebingen, Germany.*

[9]*Cluster of Excellence: EXC 2124: Controlling Microbes to Fight Infection, Tübingen, Germany.*

[10]*School of Earth Sciences, University of Bristol, UK.*

SUPPORTING INFORMATION

Number of figures in supporting information: 12

Number of tables in supporting information: 1

Total numbers of pages in supporting information: 23 (including cover page)

Synthesis of Ferrihydrite-coated Sand. Quartz sand with a grain size of 0.4-0.8 mm (Carl Roth GmbH + Co.KG, Germany) was used. The sand was pre-treated by first autoclaving the sand at 121°C for 20 minutes, followed by washing with 1 M HCl (24 h, completely covered) and finally with Aqua Regia for 5 min to further improve Fe coating efficiency by increasing the surface area, as has been done previously[1, 2]. Afterwards the sand was washed with MiliQ water and dried at 60°C.

The Fe(III) oxyhydroxide 2-line ferrihydrite (FH) was synthesized in the presence of the sand by precipitation from a $Fe(NO_3)_3$*$9H_20$ solution by adding 1 M KOH. The $Fe(NO_3)_3$*$9H_20$ solution was added to 500 g of sand and stirred manually by hand as KOH was added dropwise until a pH of 7.3 was reached. The mixture was then left without stirring. After two hours, the pH was readjusted to 7.5 and the mixture left overnight on a rolling shaker (15 rpm), as has been done previously[1]. Finally, the mixture was washed with MiliQ water and dried at 40°C to avoid temperature-induced modifications of the precipitates[1].

In the end, the fresh synthesized ferrihydrite-coated sand yielded an iron content of 2.19±0.26 mg poorly crystalline Fe(III) per g sand, determined by 0.5 M HCl extraction, performed in triplicates, followed by Fe quantification in the extract by Ferrozine assay[3]. Treating the unexposed sand in the same manner as the exposed sand (transport to the field and back, during exposure time stored at room temperature), formed a more crystalline Fe(III) phase (1.01±0.14 mg Fe(III) per g sand), which was only extractable by 6 M HCl, not extractable with 1 M Na-acetate and 0.5 M HCl. As also previously stated[1], the FH coating increased the specific surface area (SSA) from 0.07 m^2 per g of the initial pure sand to 1.49 m^2 per g of the FH-coated sand (21 times higher than for its uncoated precursor).

Exposure Bags. The FH-coated sand was packed in Teflon bags (polytetrafluoroethylene (PTFE); or Teflon®) with 0.1 mm thickness and manually pierced with needles of 0.55 mm

diameter under sterile conditions in a Biological Safety Cabinet (BSC). The bag was closed with a cable tie at the top and with a long plastic line, which was later used to mark the position of the bag at the surface and pull it out after exposure. The Teflon along with additional equipment (FH coated sand, cable ties) was autoclaved (121°C, 1 bar pressure, 20 mins) prior to use, brought into the BSC cabinet and exposed to UV-light for 15 minutes. The Teflon was chosen based on the following suitable properties: heat (up to 250°C) and cold (till -196°C) resistant; unaffected by most chemicals, especially iron; no adhesive forces and weather resistant[4, 5].

The bags filled with FH-coated sand were stored at room temperature in sterile plastic bags and transported to the field under sterile conditions.

Sequential Fe Extraction. 0.5 g of homogenized sand of each thaw stage and exposure time was added under anoxic conditions (100% N_2, remaining O_2 <100 ppm) into Eppendorf tubes. As previously described[6], samples were centrifuged (5 min, 12,000 g) and the porewater (supernatant) was removed. 1 mL of anoxic 1 M Na-acetate solution was added to the pellet, mixed and incubated for 24 h in the dark. Then, the sample was centrifuged (5 min, 12,000 g) and the supernatant was collected and stored anoxically in the dark at 4°C until further analysis. To the pellet, 1 mL of anoxic 0.5 M HCl was added, mixed and incubated in the dark under anoxic conditions for 2 h. After centrifugation again, the supernatant was removed and stored anoxically at 4°C until further analysis. To the remaining pellet, 1 mL of anoxic 6 M HCl was added, mixed and incubated for 24 h in the dark as the last extraction step[6]. The supernatant was again stored under anoxic conditions in the dark at 4°C until further analysis.

Scanning Electron Microscopy (SEM) and Energy Dispersive X-Ray Analysis (EDS). The sand of the reference material (unexposed FH-coated sand) and the homogenized sand of each

thaw stage for two months exposure (palsa, bog and fen) were anoxically dried (24 h, 100% N_2 atmosphere). After reaching constant weight, the dried sand was pressed in an indium band (Plano GmbH, article number: E432), specifically chosen to avoid a carbon background signal in the EDS analysis. The indium band was then glued to the SEM sample stub with conductive silver paint (ACHESON Silver DAG 141; Plano GmbH, article number: G3692). After a short drying time (5 min), the samples were immediately coated with ~8 nm Pt-layer using a BAL-TEC SCD 500 sputter coater, operated in a working distance of 35 mm, for 90 seconds at 0.02 mbar. SEM and EDS analysis were performed at the Center for Applied Geosciences, University Tuebingen, using a Zeiss Crossbeam 550L Cryo-FIB-SEM, equipped with an Oxford EDS detector (UltimMax 100) and AZtecEnergy Advanced software. SEM images were acquired at a working distance of 5 mm by use of the Secondary Electrons Secondary Ions (SESI) detector using an acceleration voltage of 30 kV during the EDS analysis session and at 5 kV (for images about surface information) with a 39x, 250x and 650x magnification and a store resolution of 2048 pixel image width. Four replicates per sample were analyzed.

The EDS analysis was performed at a working distance of 5 mm, with a probe current of 200pA, 2048 channels, process time 6, Acquisition mode: Live time and Acquisition time of 470 live seconds.

Microbial Community Analysis. After using the PowerSoil® RNA and DNA isolation kit, DNA samples were eluted in 50 µl RNase/DNase-Free water. DNA concentrations were determined using a Qubit® 2.0 Fluorometer with DNA HS kit (Life Technologies, Carlsbad, CA, USA). Quantitative PCR (qPCR) specific for the 16S rRNA (gene) of bacteria and archaea was performed as described previously[7]. Microbial 16S rRNA (genes) were amplified using primers 515F and 806R[8]. Quality and quantity of the purified amplicons were determined using agarose gel electrophoresis and Nanodrop (NanoDrop 1000, Thermo Scientific, Waltham, MA, USA). Subsequent library preparation steps (Nextera, Illumina) and sequencing were

performed by Microsynth AG (Switzerland) using the 2 × 250 bp MiSeq Reagent Kit v2 on an Illumina MiSeq sequencing system (Illumina, San Diego, CA, USA). From 113,554 to 151,092 (average 135,126) read pairs were generated per sample. Quality control, reconstruction of 16S rRNA (gene) sequences and taxonomic annotation was performed with nf-core/ampliseq v1.1.2[9, 10] with Nextflow v20.10.0[11] using containerized software with singularity v3.4.2[12]. Primers were trimmed, and untrimmed sequences were discarded (< 13%, on average 9.6%) with Cutadapt v2.6[13]. Adapter and primer-free sequences were imported into QIIME2 version 2019.10.0[14], processed with DADA2 version 1.10.0[15] to eliminate PhiX contamination, trim reads (before the median quality drops below 38, i.e. position 137 in forward reads and 194 in reverse reads), correct errors, merge read pairs, and remove PCR chimeras; ultimately, in total 937 amplicon sequencing variants (ASVs) were obtained across all samples. Alpha rarefaction curves were produced with the QIIME2 diversity alpha-rarefaction plugin, which indicated that the richness of the samples had been fully observed. A Naive Bayes classifier was fitted with 16S rRNA (gene) sequences extracted with the PCR primer sequences from the QIIME compatible, 99%-identity clustered SILVA v132 database[16]. ASVs were classified by taxon using the fitted classifier[17]. 45 ASVs that classified as chloroplasts or mitochondria were removed, totalling to < 0.5% (average 0.36%) relative abundance per sample, and the remaining 892 ASVs had their abundances extracted by feature-table (https://github.com/qiime2/q2-feature-table).

DNA extraction was only successful for the long-term exposed bags in the fully-thawed fen.

Isolation of Fe(III)-reducing bacteria was performed with anoxic media and supplies (5 mM acetate and 5 mM lactate) via multiple rounds of extinction, as previously described[18]. The headspace in the dilution series was N_2:CO_2 (90:10). To the first tube of a dilution series, 1g of FH-coated sand was added, and a 10x dilution series up to a dilution of 10^{-12} was prepared. To identify the isolated Fe(III)-reducing bacteria, DNA was extracted of the isolated culture (after

ten transfers) using the UltraClean® Microbial DNA Isolation Kit (MO BIO Laboratories, Carlsbad, CA, US). Then, 16S rRNA gene fragments were amplified using the 341F (CCTACGGGAGGCAGCAG) and 907R (CCGTCAATTCCTTTRAGTTT) primer pair and resulting amplicons were sent for Sanger sequencing (Eurofins GATC biotech, Konstanz, Germany). Sequence results (deposited at database) were analyzed using nucleotide Basic Local Alignment Search Tool (BLAST) to identify the closest relative (performed on the 20th of April 2021, algorithm: blastn, standard database: nucleotide collection (nr/nt), accession number: Y19190.1; see also Figure S5).

Redox Potential Analysis. Redox potential at redox potential probes was recorded every 30 seconds by a datalogger (CR1000, Campbell Scientific) and averaged over 10 minutes. For this study, the reported values at each time point represent the average (± standard error) of values recorded at 6, 8, and 10 cm. In the bog and fen, the values across the two probes were averaged. Redox potential was referenced to two Ag^0/AgCl reference electrodes deployed within the bog and fen. Retrieved data were adjusted to the standard hydrogen electrode (SHE) by adding 213 mV to the recorded values as recommended by the provider company (PaleoTerra).

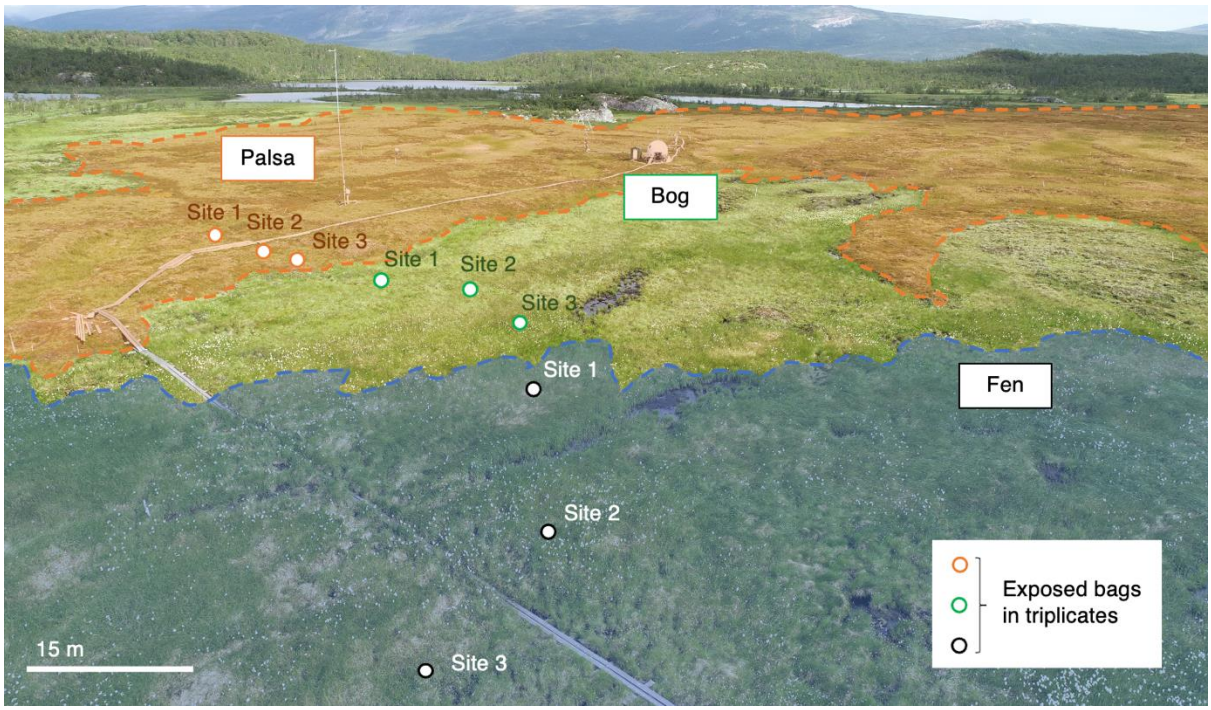

Figure S1. Sites for exposure of the bags with ferrihydrite-coated sand along the thaw gradient from palsa (intact) to bog (partially-thawed) to fen (fully-thawed) at Stordalen mire, Abisko (Sweden). Orange background marks the palsa, green the bog and blue the fen areas. At each thaw stage (palsa: 68°21'18.91"N, 19° 2'38.02"E to 68°21'18.78"N, 19° 2'39.18"E, bog: 68°21'18.86"N 19° 2'39.94"E to 68°21'18.35"N, 19° 2'40.39"E, fen: 68°21'18.01"N, 19° 2'40.08"E to 68°21'17.38"N, 19° 2'38.99"E), three sites were chosen following the hydrology flow[19]. For the short-term exposure, we exposed three replicate bags of ferrihydrite-coated sand for two weeks during early summer (nine bags per thaw stage in total). For the longer-term exposure of two months, triplicate bags were exposed at the centered positions of each thaw stage to capture conditions characteristic for each thaw stage: palsa site 1, bog site 2 and fen site 2, resulting in three replicate bags per thaw stage.

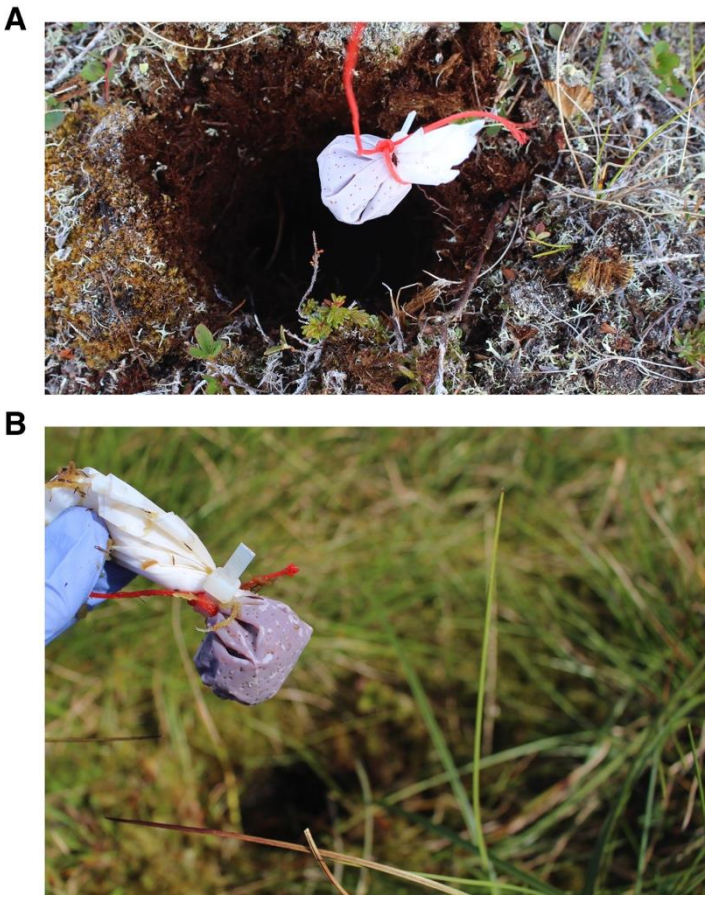

Figure S2. Examples of ferrihydrite-coated sand in teflon bags exposed in intact palsa (A) and fully-thawed fen (B). Each bag was placed at 10 cm depth and the hole was re-sealed with the soil layer which had been removed.

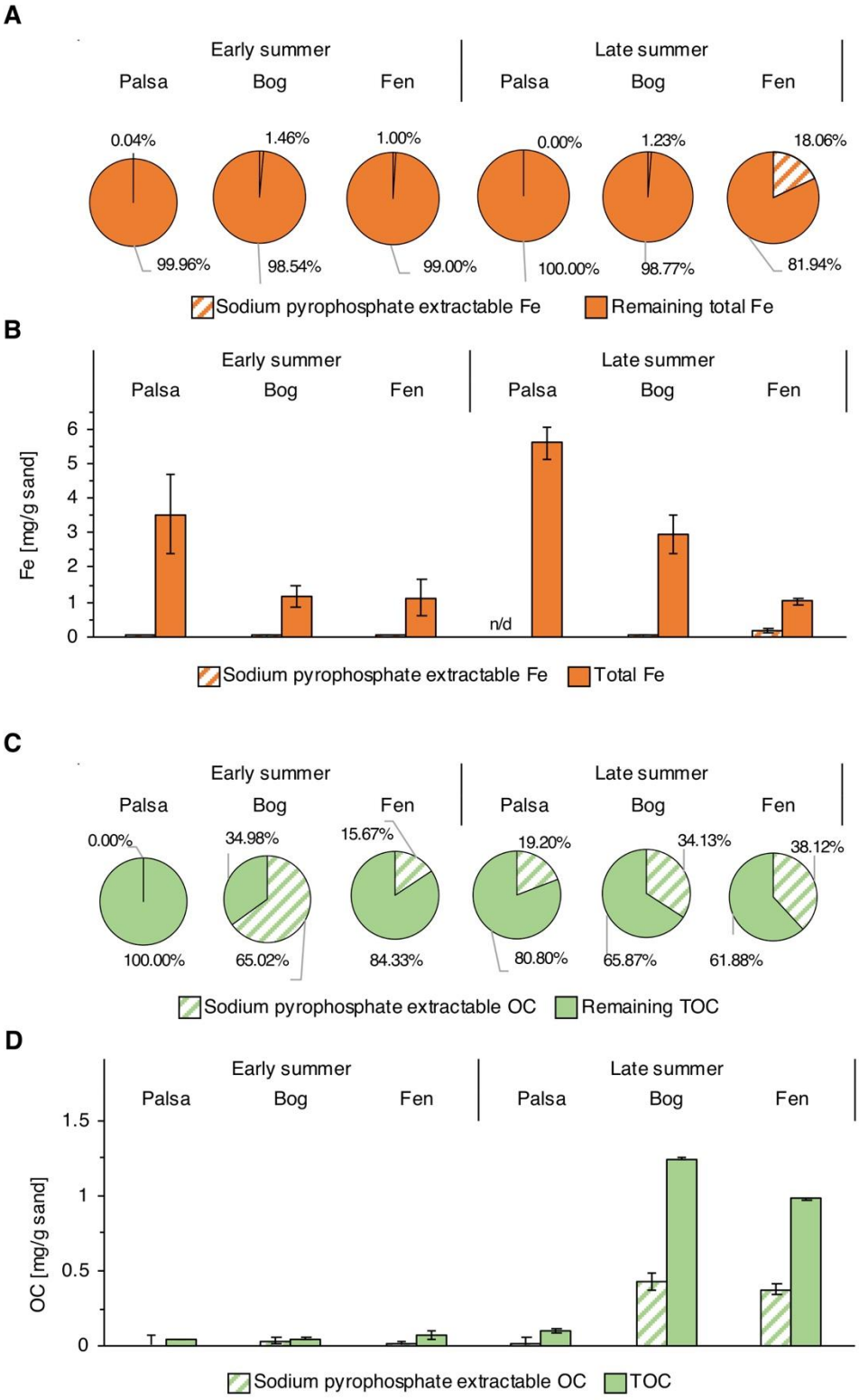
A
Early summer
Late summer
Palsa
Bog
Fen
Palsa
Bog
Fen
0.04%
1.46%
1.00%
0.00%
1.23%
18.06%
99.96%
98.54%
99.00%
100.00%
98.77%
81.94%
Sodium pyrophosphate extractable Fe
Remaining total Fe
B
Early summer
Late summer
Palsa
Bog
Fen
Palsa
Bog
Fen
Fe [mg/g sand]
0
1
2
3
4
5
6
n/d
Sodium pyrophosphate extractable Fe
Total Fe
C
Early summer
Late summer
Palsa
Bog
Fen
Palsa
Bog
Fen
0.00%
34.98%
15.67%
19.20%
34.13%
38.12%
100.00%
65.02%
84.33%
80.80%
65.87%
61.88%
Sodium pyrophosphate extractable OC
Remaining TOC
D
Early summer
Late summer
Palsa
Bog
Fen
Palsa
Bog
Fen
OC [mg/g sand]
0
0.5
1
1.5
Sodium pyrophosphate extractable OC
TOC

892

Figure S3. Sodium pyrophosphate extractable iron (Fe) and organic carbon (OC) versus total Fe and TOC along the thaw gradient until early summer (2 weeks exposure) and until late summer (2 months exposure). (A) Colloidal/OM-chelated Fe (defined as sodium pyrophosphate extractable Fe) (in orange lines) [% of the total Fe content associated with sand (in orange)] along the thaw gradient with time. (B) Absolute amounts of sodium pyrophosphate extractable Fe and total Fe along the thaw gradient with time. (C) Sodium pyrophosphate extractable OC (in green lines) [% of the TOC associated with sand (in green)] along the thaw gradient with time. (D) Absolute amounts of sodium pyrophosphate extractable OC and TOC along the thaw gradient with time. Reported values for the early summer period are the average and error bars are the standard deviation of triplicate analysis of nine homogenized bags, which were exposed at each thaw stage (palsa, bog and fen). Reported values for the late summer period are the average and error bars are the standard deviation of triplicate analysis of three homogenized bags, exposed at each thaw stage. n/d = not detected.

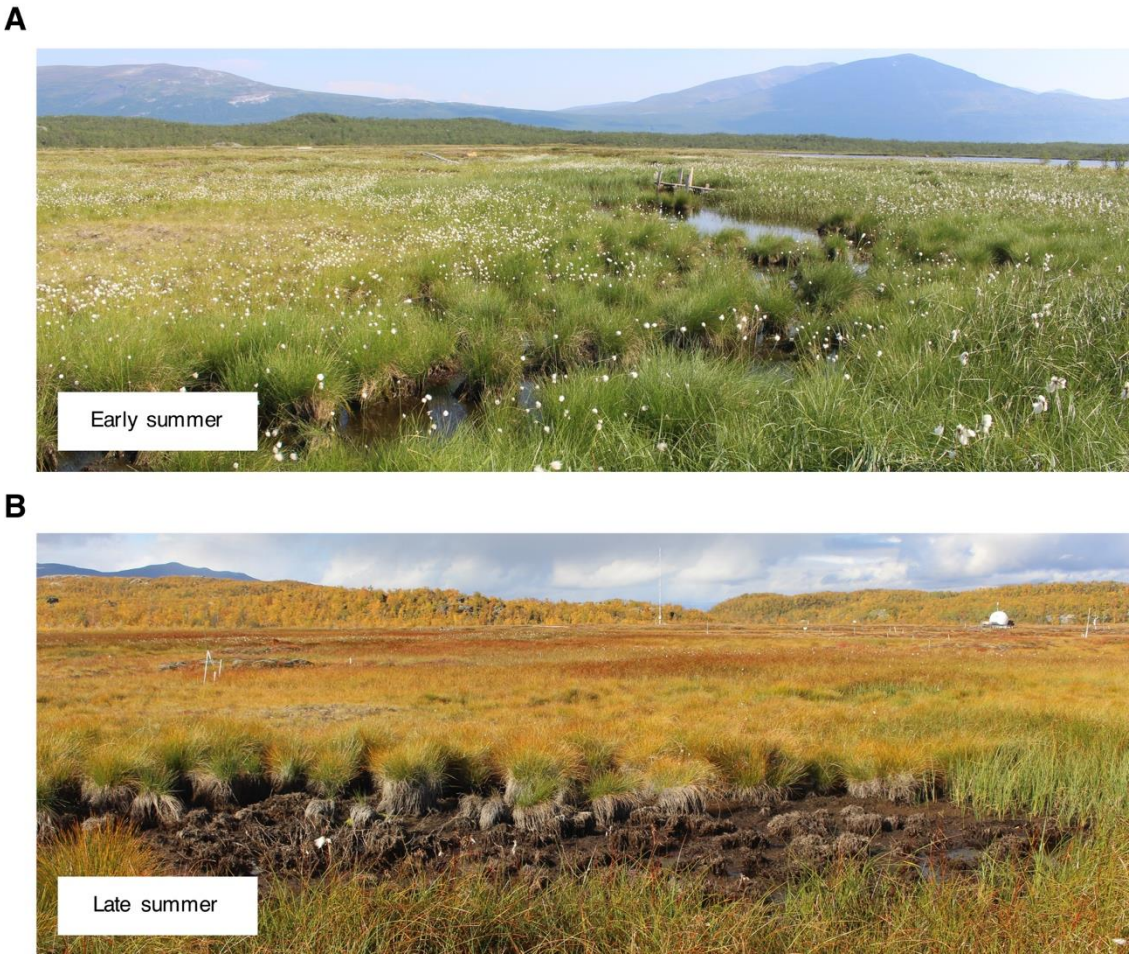

Figure S4. Seasonal changes at Stordalen mire in early summer (A) and late summer (B). In early summer, the semi-wet bog and waterlogged fen areas were completely water-saturated. During summer, bog areas became drier due to increasing drainage caused by active layer deepening and decreasing volumetric soil water content in the upper 10 cm.

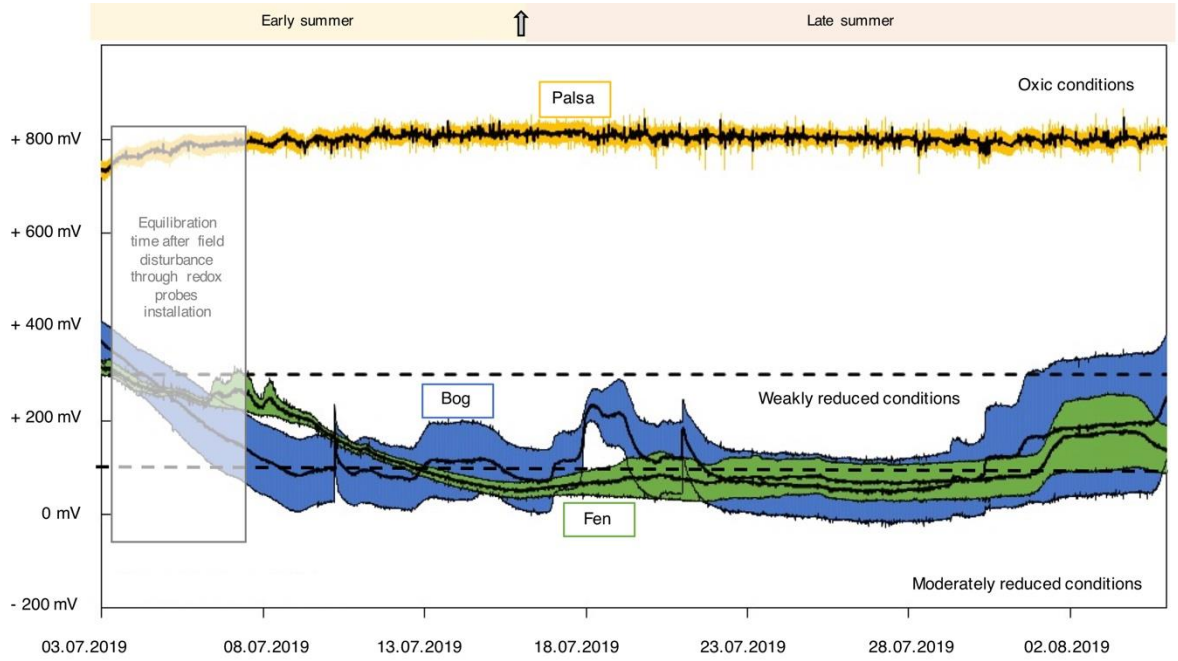

916

917

918 **Figure S5. Redox potential along the thaw gradient.** Black lines report the average redox
919 potential [mV] and the colored areas represent the standard deviation across the three depths at
920 6, 8 and 10 cm in each thaw stage. The redox potential measured in palsa is marked in yellow,
921 in bog in blue and in fen in green. The first 1-2 days represent the equilibrium phase after
922 installing the redox probes in the field. Values above +300 mV are considered as oxic
923 conditions. Values of +300 mV to +100 mV are considered as weakly reduced and values of
924 +100 to -100 mV as moderately reducing conditions[20]. Towards August, the redox potential in
925 bog increases from 0 mV to above +300 mV which marks a potential shift from Fe(III)-reducing
926 to Fe(II)-oxidizing conditions. Unfortunately, the redox probes disconnected from the battery
927 in mid-August and remote data collection ceased.

928

929

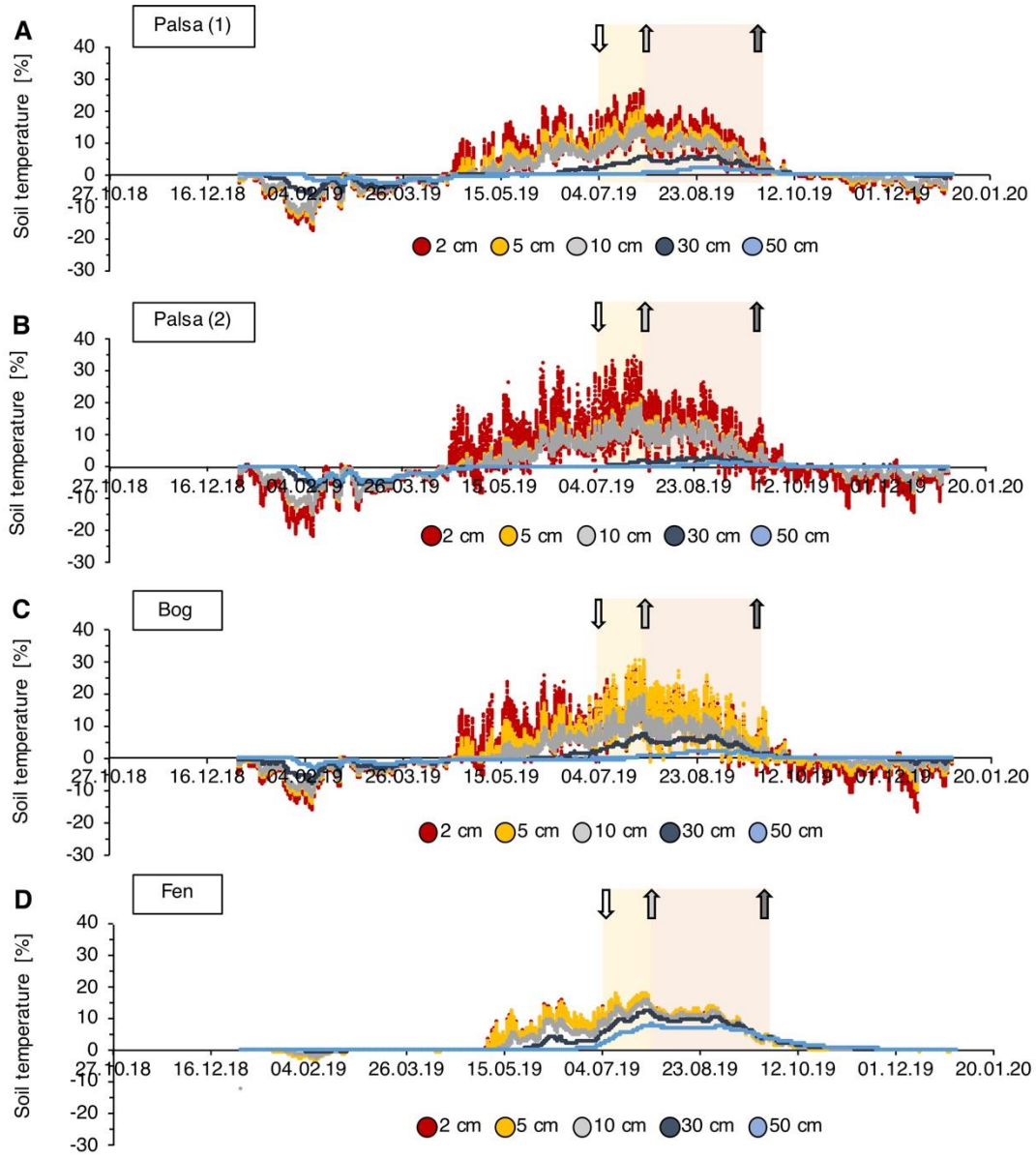

930

931

932 **Figure S6. Soil temperatures at each thaw stage at 2 cm, 5 cm, 10 cm, 30 cm and 50 cm**
933 **soil depth: (A) palsa (replicate 1; 68°21'22.25"N, 19° 2'42.22"E), (B) palsa (replicate 2;**
934 **68°21'21.05"N, 19° 2'38.85"E), (C) bog (68°21'20.49"N, 19° 2'45.52"E) and (D) fen**
935 **(68°21'20.20"N, 19° 2'42.37"E) in the year 2019[21].**

936

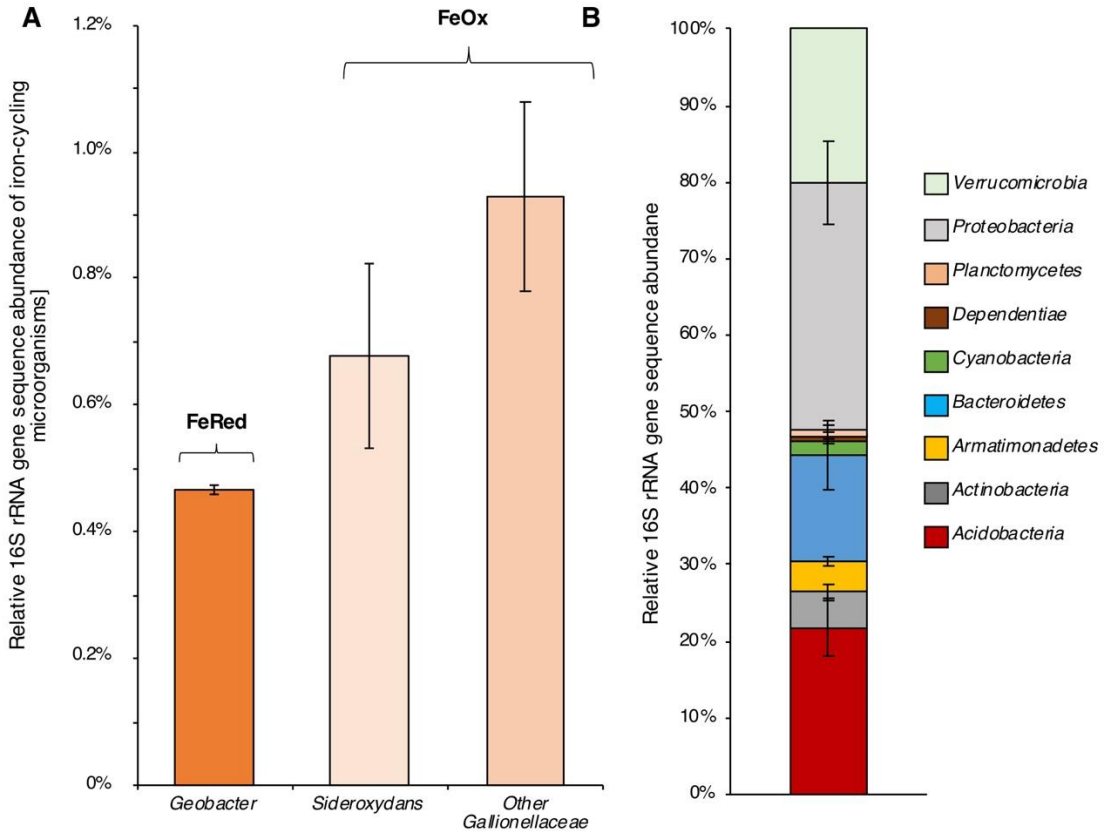

Figure S7. Microbial community of ferrihydrite-coated sand exposed for 2 months in the fully-thawed fen till late summer. (A) Detected microbial iron-metabolizing key players: Fe(III)-reducing bacteria (FeRed) and Fe(II)-oxidizing bacteria (FeOx). (B) Present microbial community. Values and error bars represent average and standard deviation of triplicate 16S rRNA gene amplicon sequencing abundance analysis of homogenized ferrihydrite-coated sand exposed in fully-thawed fen from early to late summer.

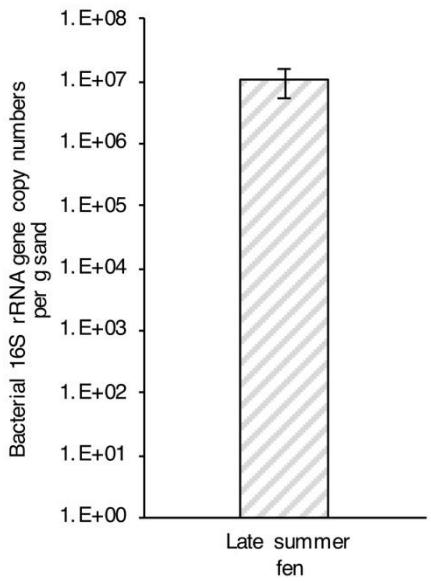

946

947

948 **Figure S8. Bacterial 16S rRNA gene copy numbers based on qPCR analysis** of the
949 homogenized ferrihydrite-coated sand exposed for 2 months in the fully-thawed fen till late
950 summer.

951

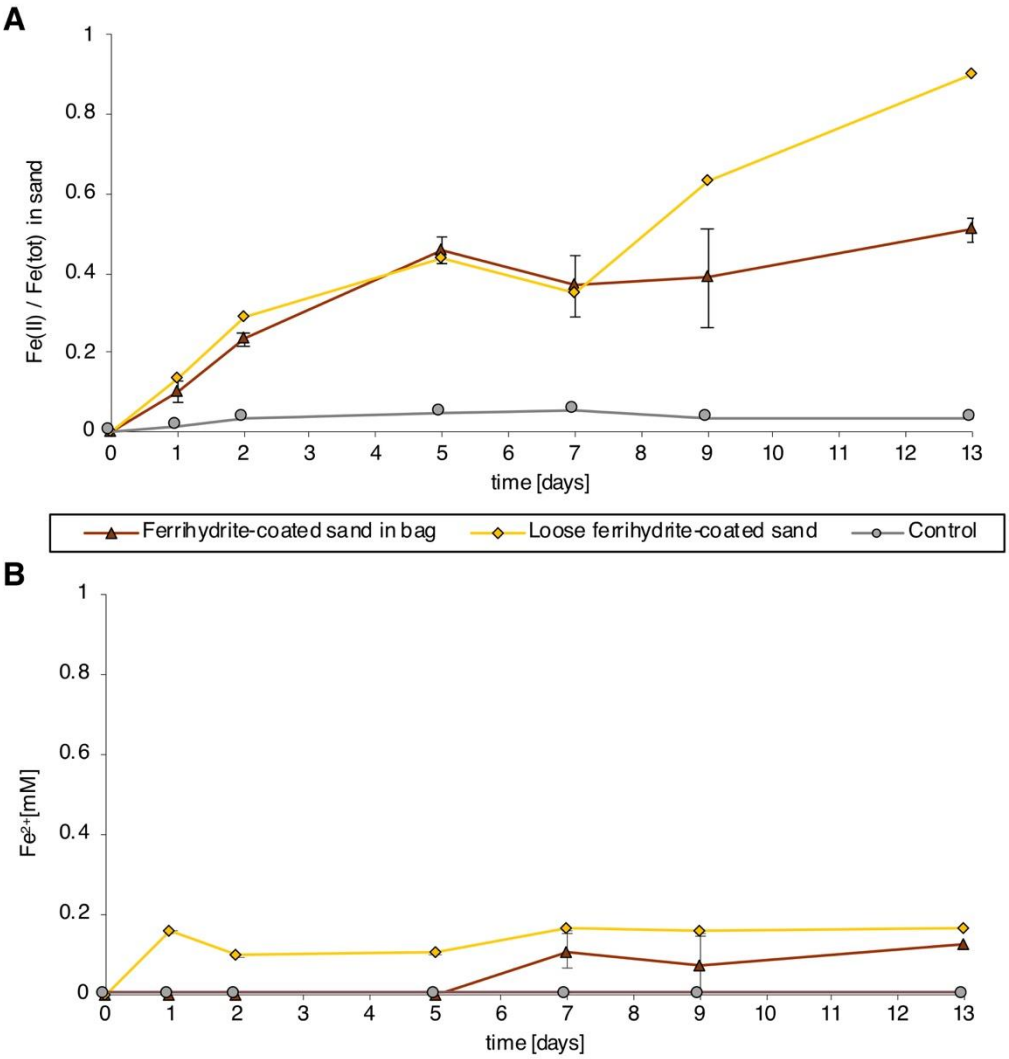

952

953

954 **Figure S9. Microbial Fe(III) reduction under lab conditions in loose ferrihydrite-coated**
955 **sand versus ferrihydrite-coated sand in teflon bags.** (A) Fe(II)/Fe(tot) ratio in sand over 13
956 days in anoxic fresh water media, containing 5 mM acetate, 2 mM cysteine and inoculated with
957 *Geobacter metallidurans* (10^8 cells/mL). Reported values represent the average and range of
958 duplicates of each setup. Yellow shows the Fe(II)/Fe(tot) ratio during reduction of loose
959 ferrihydrite-coated sand over time. Brown shows the Fe(II)/Fe(tot) ratio in setups with
960 ferrihydrite-coated sand in teflon bags over time. Control represents data for incubation of loose
961 ferrihydrite-coated sand without *Geobacter metallidurans* inoculum. An Fe(II)/Fe(tot) ratio of
962 1 means 100% Fe(II) formation in the sand phase. (B) Only low concentrations of dissolved
963 Fe^{2+} (below 0.2 mM) were present in the liquid phase.

964

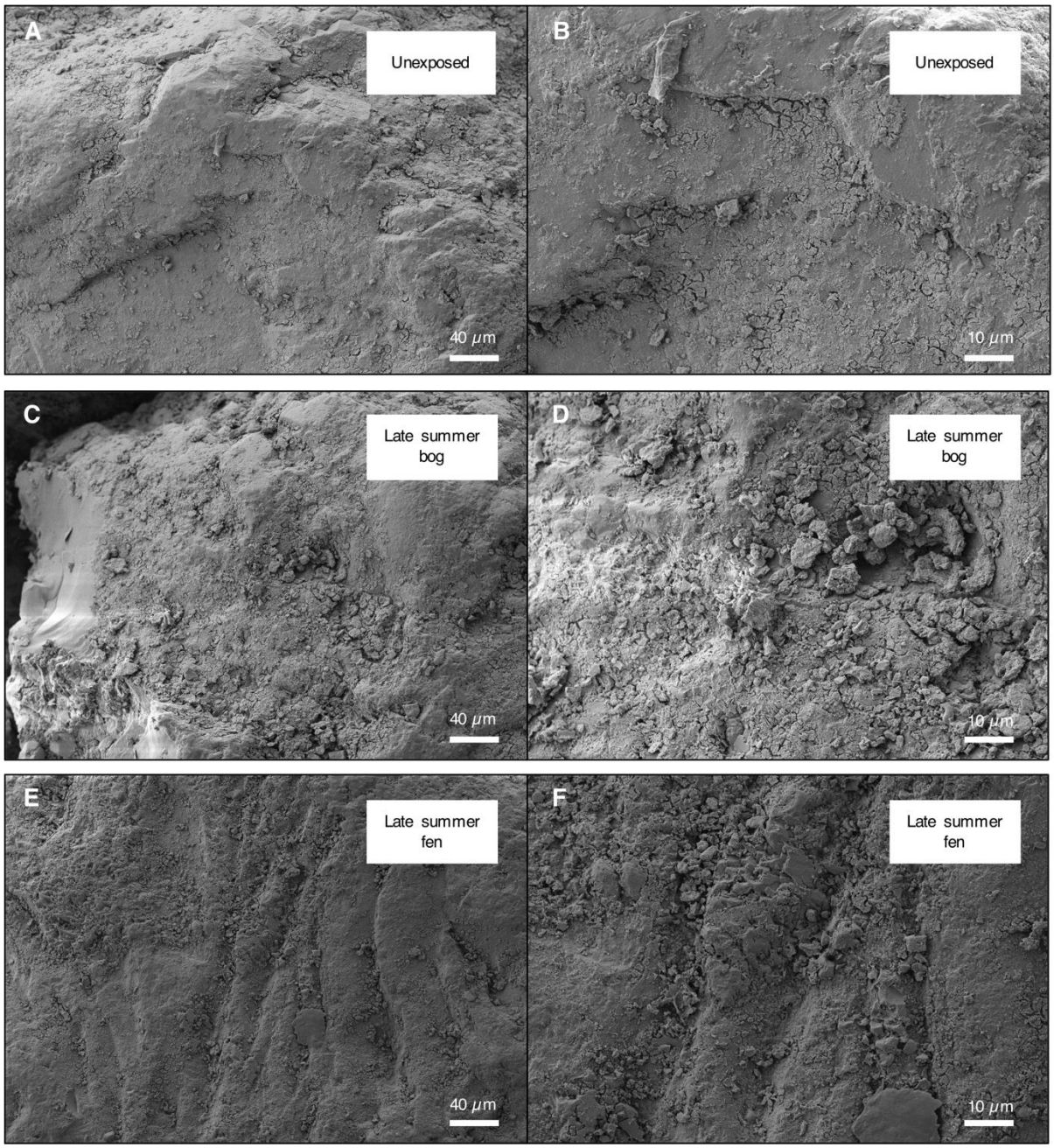

Figure S10. Scanning electron microscopy surface analysis of the ferrihydrite-coated sands before and after exposure. Unexposed sand shows smooth surfaces and small aggregate formation on the sand grains: (A) overview image and (B) close up image of unexposed sand. Ferrihydrite-coated sand exposed for 2 months till late summer in the partially-thawed bog shows aggregate formation on the surface of the sand grains: (C) overview image and (D) close up image of sand exposed for 2 months till late summer in the partially-thawed bog (replicate analysis to Figure 4 shown in the main text). Ferrihydrite-coated sand exposed for 2 months till late summer in the fully-thawed fen shows aggregate formation on the sand grains surface: (E) overview image and (F) close up image of sand exposed till late summer in the fully-thawed fen.

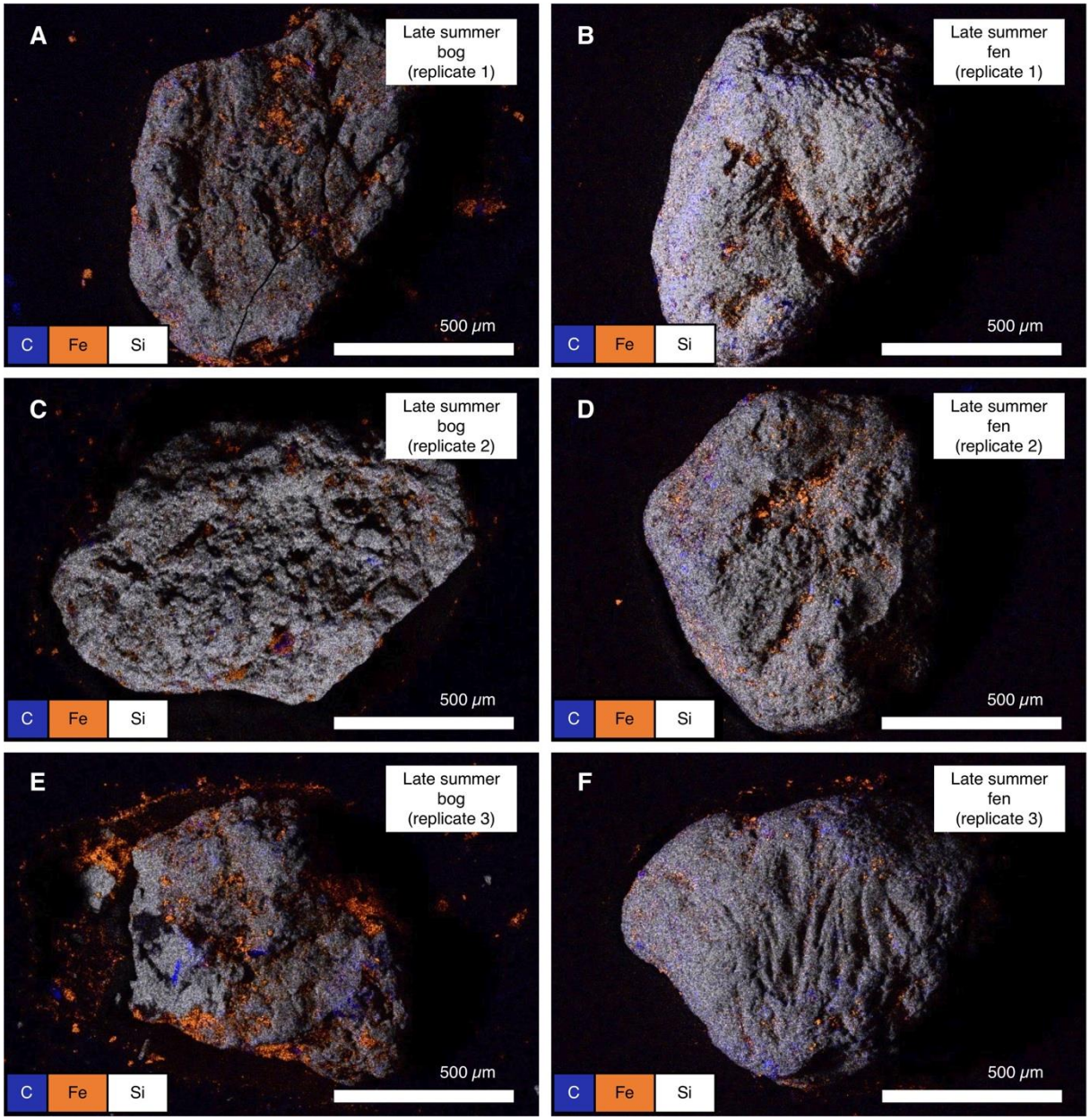

Figure S11. EDS derived chemical distribution maps of the replicate analysis of iron (Fe)-organic carbon (OC) associations at the surface of the ferrihydrite-coated sand grains exposed in partially-thawed bog and fully-thawed fen collected after exposure for 2 months till late summer: (A) and (B) replicate 1, (C) and (D) replicate 2, (E) and (F) replicate 3.

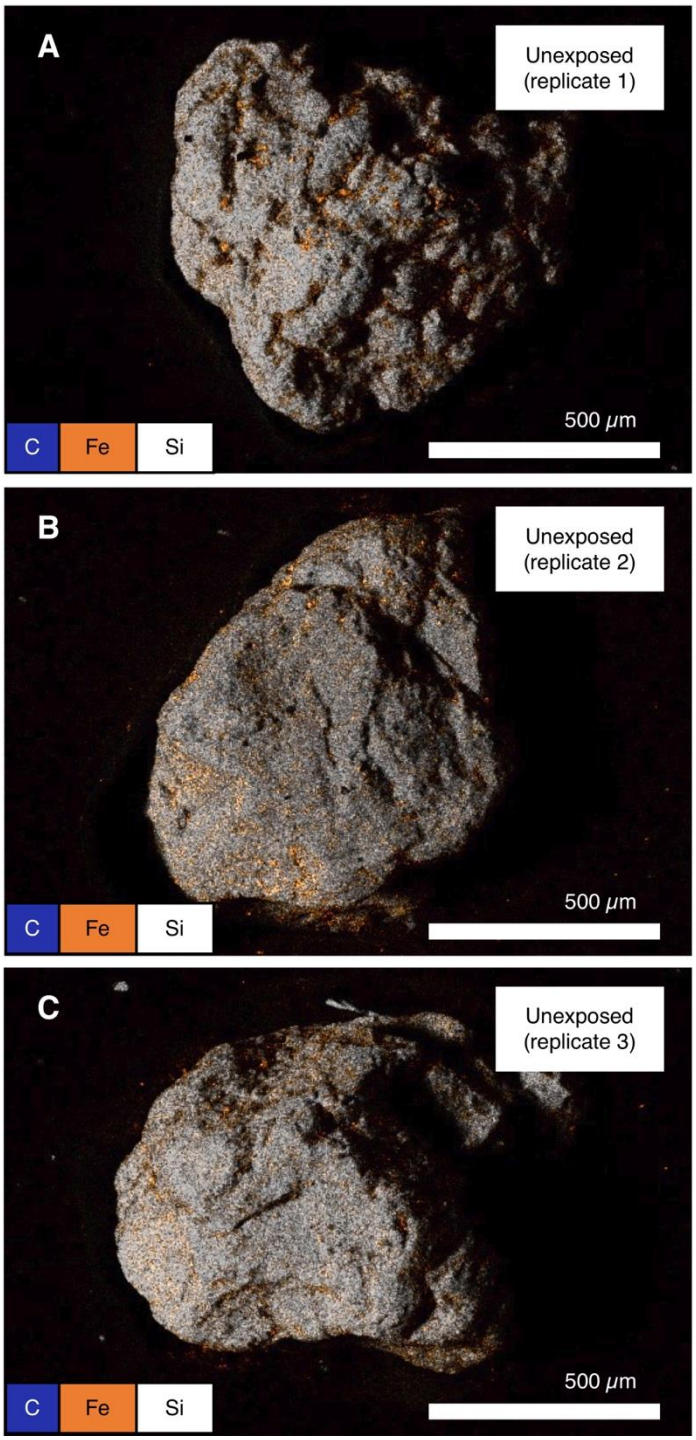

984

985 **Figure S12. EDS derived chemical distribution maps of iron (Fe) coating on unexposed**
986 **ferrihydrite-coated sand grains: (A) replicate 1, (B) replicate 2 and (C) replicate 3.**

987

988 **Table S1. Organic carbon (OC) to iron (Fe) ratios in the active layer of the partially**
989 **thawed bog and in the fully-thawed fen collected after exposure of 2 months till late**
990 **summer.**

		Total extractable OC and Fe	Fe-bound OC*
		TOC/totalFe (wt:wt)	OC/Fe (wt:wt)
Late summer	Bog	0.42	0.28
	Fen	0.96	0.73
		TOC/total Fe (molar ratio)	OC/Fe (molar ratio)
Late summer	Bog	1.96	1.31
	Fen	4.47	3.38

991 *(TOC-sodiumpyrophosphate extractable OC)/(total Fe-sodium pyrophosphate extractable Fe)

992

References:

1. Sorwat, J.; Mellage, A.; Kappler, A.; Byrne J. M. Immobilizing magnetite onto quartz sand for chromium remediation. *Journal of Hazardous Materials* **2020,** *400*, 123139.

2. Kango, S.; Kumar, R. Magnetite nanoparticles coated sand for arsenic removal from drinking water. *Environ Earth Sci* **2016,** *75*, (5), 381.

3. Stookey, L. L. Ferrozine - a New Spectrophotometric Reagent for Iron. *Anal Chem* **1970,** *42*, (7), 779-781.

4. Biswas, S.; Vijayan, K. Friction and wear of ptfe - a review. *Wear* **1992,** *158*, 193-211.

5. Buerkle, M.; Asai, Y. Thermal conductance of teflon and polyethylene: insight from an atomistic, single-molecule level. *Sci Rep* **2017,** *7*, 41898 .

6. Lueder, U.; Maisch, M.; Laufer, K.; Jorgensen, B.B.; Kappler, A.: Schmidt, C. Influence of physical pertubation on Fe(II) supply in coastal marine sediments. *Environ Sci Technol* **2020,** *54*, 3209-3218.

7. Otte, J. M.; Harter, J.; Laufer, K.; Blackwell, N.; Straub, D.; Kappler, A.; Kleindienst, S., The distribution of active iron-cycling bacteria in marine and freshwater sediments is decoupled from geochemical gradients. *Method Enzymol* **2018,** *20*, (7), 2483-2499.

8. Caporaso, J. G.; Kuczynski, J.; Stombaugh, J.; Bittinger, K.; Bushman, F. D.; Costello, E. K.; Fierer, N.; Pena, A. G.; Goodrich, J. K.; Gordon, J. I.; Huttley, G. A.; Kelley, S. T.; Knights, D.; Koenig, J. E.; Ley, R. E.; Lozupone, C. A.; McDonald, D.; Muegge, B. D.; Pirrung, M.; Reeder, J.; Sevinsky, J. R.; Tumbaugh, P. J.; Walters, W. A.; Widmann, J.; Yatsunenko, T.; Zaneveld, J.; Knight, R. QIIME allows analysis of high-throughput community sequencing data. *Nat Methods* **2010,** *7*, (5), 335-336.

9. Ewels, P. A.; Peltzer, A.; Fillinger, S.; Patel, H.; Alneberg, J.; Wilm, A.; Garcia, M. U.; Di Tommaso, P.; Nahnsen, S. The nf-core framework for community-curated bioinformatics pipelines. *Nat Biotechnol* **2020,** *38*, (3), 276-278.

10. Straub, D.; Blackwell, N.; Langarica-Fuentes, A.; Peltzer, A.; Nahnsen, S.; Kleindienst, S. Interpretations of environmental microbial community studies are biased by the selected 16S rRNA (gene) amplicon sequencing pipeline. *Front Microbiol* **2020,** *11*, 550420.

11. Di Tommaso, P.; Chatzou, M.; Floden, E. W.; Barja, P. P.; Palumbo, E.; Notredame, C. Nextflow enables reproducible computational workflows. *Nat Biotechnol* **2017,** *35*, (4), 316-319.

12. Kurtzer, G. M.; Sochat, V.; Bauer, M. W. Singularity: Scientific containers for mobility of compute. *PLoS One* **2017,** *12*, (5), e0177459.

13. Martin, M. Cutadapt removes adapter sequences from high-throughput sequencing reads. *EMBnet journal* **2011,** *17*, (1), 3.

14. Bolyen, E.; Rideout, J. R.; Dillon, M. R.; Bokulich, N. A.; Abnet, C. C.; Al-Ghalith, G. A.; Alexander, H.; Alm, E. J.; Arumugam, M.; Asnicar, F.; Bai, Y.; Bisanz, J. E.; Bittinger, K.; Brejnrod, A.; Brislawn, C. J.; Brown, C. T.; Callahan, B. J.; Caraballo-Rodríguez, A. M.; Chase,

J.; Cope, E. K.; Da Silva, R.; Diener, C.; Dorrestein, P. C.; Douglas, G. M.; Durall, D. M.; Duvallet, C.; Edwardson, C. F.; Ernst, M.; Estaki, M.; Fouquier, J.; Gauglitz, J. M.; Gibbons, S. M.; Gibson, D. L.; Gonzalez, A.; Gorlick, K.; Guo, J.; Hillmann, B.; Holmes, S.; Holste, H.; Huttenhower, C.; Huttley, G. A.; Janssen, S.; Jarmusch, A. K.; Jiang, L.; Kaehler, B. D.; Kang, K. B.; Keefe, C. R.; Keim, P.; Kelley, S. T.; Knights, D.; Koester, I.; Kosciolek, T.; Kreps, J.; Langille, M. G. I.; Lee, J.; Ley, R.; Liu, Y. X.; Loftfield, E.; Lozupone, C.; Maher, M.; Marotz, C.; Martin, B. D.; McDonald, D.; McIver, L. J.; Melnik, A. V.; Metcalf, J. L.; Morgan, S. C.; Morton, J. T.; Naimey, A. T.; Navas-Molina, J. A.; Nothias, L. F.; Orchanian, S. B.; Pearson, T.; Peoples, S. L.; Petras, D.; Preuss, M. L.; Pruesse, E.; Rasmussen, L. B.; Rivers, A.; Robeson, M. S., 2nd; Rosenthal, P.; Segata, N.; Shaffer, M.; Shiffer, A.; Sinha, R.; Song, S. J.; Spear, J. R.; Swafford, A. D.; Thompson, L. R.; Torres, P. J.; Trinh, P.; Tripathi, A.; Turnbaugh, P. J.; Ul-Hasan, S.; van der Hooft, J. J. J.; Vargas, F.; Vázquez-Baeza, Y.; Vogtmann, E.; von Hippel, M.; Walters, W.; Wan, Y.; Wang, M.; Warren, J.; Weber, K. C.; Williamson, C. H. D.; Willis, A. D.; Xu, Z. Z.; Zaneveld, J. R.; Zhang, Y.; Zhu, Q.; Knight, R.; Caporaso, J. G. Reproducible, interactive, scalable and extensible microbiome data science using QIIME 2. *Nat Biotechnol* **2019,** *37*, (8), 852-857.

15. Callahan, B. J.; McMurdie, P. J.; Rosen, M. J.; Han, A. W.; Johnson, A. J.; Holmes, S. P. DADA2: High-resolution sample inference from Illumina amplicon data. *Nat Methods* **2016,** *13*, (7), 581-3.

16. Pruesse, E.; Quast, C.; Knittel, K.; Fuchs, B. M.; Ludwig, W.; Peplies, J.; Glockner, F. O. SILVA: a comprehensive online resource for quality checked and aligned ribosomal RNA sequence data compatible with ARB. *Nucleic Acids Res* **2007,** *35*, (21), 7188-96.

17. Bokulich, N. A.; Kaehler, B. D.; Rideout, J. R.; Dillon, M.; Bolyen, E.; Knight, R.; Huttley, G. A.; Gregory Caporaso, J. Optimizing taxonomic classification of marker-gene amplicon sequences with QIIME 2's q2-feature-classifier plugin. *Microbiome* **2018,** *6*, (1), 90.

18. Patzner, M. S., Mueller, C. W., Malusova, M., Baur, M., Nikeleit, V., Scholten, T., Hoeschen, C., Byrne, J. M., Borch, Thomas, Kappler, A. & C. Bryce, Iron mineral dissolution releases iron and associated organic carbon during permafrost thaw. Nat Commun 11, 6329 (2020).

19. Olefeldt, D.; Roulet, N. T. Effects of permafrost and hydrology on the composition and transport of dissolved organic carbon in a subarctic peatland complex. *J Geophys Res-Biogeo* **2012,** *117*, G01005.

20. Reddy, K. R.; DeLaune, R.D. Biogeochemistry of wetlands: Science and applications. *CRC Press, Boca Raton, FL.* **2008**, ISBN 978-1-56670-678-0.

21. Rinne, J., ICOS Sweden Ecosystem eco time series (ICOS Sweden), Abisko-Stordalen Palsa Bog, 2018-12-31–2019-12-31, https://hdl.handle.net/11676/s5oBzukX_FaXpHU___86QasO) **2021**.